A stable, high-order method for three-dimensional, bounded-obstacle, acoustic scattering

Qirong Fang [a,1], David P. Nicholls [b,*,2], Jie Shen [a,1]

[a] *Department of Mathematics, Purdue University, West Lafayette, IN 47907, USA*
[b] *Department of Mathematics, Statistics, and Computer Science, University of Illinois at Chicago, Chicago, IL 60607, USA*

Abstract

An efficient and high-order algorithm for three-dimensional bounded obstacle scattering is developed. The method is a non-trivial extension of recent work of the authors for two-dimensional bounded obstacle scattering, and is based on a boundary perturbation technique coupled to a well-conditioned high-order spectral-Galerkin solver. This boundary perturbation approach is justified by rigorous theoretical results on analyticity of the scattered field with respect to boundary variations which show that, in fact, the domain of analyticity can be extended to a neighborhood of the entire real axis. The numerical method is augmented by Padé approximation techniques to access this region of extended analyticity so that configurations which are large deformations of the base (spherical) geometry can be simulated. Several numerical results are presented to exemplify the accuracy, stability, and versatility of the proposed method.
© 2006 Elsevier Inc. All rights reserved.

Keywords: Acoustic scattering; High-order methods; Boundary perturbation methods; Spectral-Galerkin methods

1. Introduction

The fast and accurate numerical approximation of scattering returns from irregular obstacles is of vital importance in many problems of physical interest, e.g. non-destructive testing, spectroscopy, remote sensing, and radar imaging. There are many algorithms available for such simulations including finite differences, finite elements, and boundary integral/boundary element methods; see, e.g., the book of Colton and Kress [1], and the survey papers of Warnick and Chew [2] and Reitich and Tamma [3]. A class of methods which are both efficient and robust for a wide variety of configurations are those based upon boundary perturbations. In a recent paper [4], two of the authors presented a spectral-Galerkin/boundary perturbation method for computing scattering returns from two-dimensional irregular bounded obstacles. This method was shown to be

---

efficient (with "optimal" storage and operation counts for a method which recovers the *entire* near-field), numerically stable (with respect to *all* numerical parameters including both spatial and perturbation refinement), and highly effective for problems of low to moderate frequency (while being applicable to high frequency configurations, though not specially designed for such purposes, cf. [5]). In this paper, we discuss the implementation and performance issues surrounding the generalization of this method to the case of three-dimensional acoustic scattering where the scalar Helmholtz equation still governs the field; electromagnetic waves in three dimensions are governed by the full Maxwell equations and merit a separate investigation.

This generalization to three dimensions is non-trivial for several reasons. First, the physics of this problem are not the same as that of the two-dimensional problem as reflected, for example, in the different nature of the fundamental solution [1]. Additionally, the natural angular basis functions are now the spherical harmonics, rather than the familiar complex exponentials which appear in two dimensions, adding considerable complexity to the implementation of these algorithms. Finally, a new solver has to be developed for the resulting two-point boundary value problem which arises in the radial direction (see Section 4). However, despite these differences we have found that an implementation in three-dimensional cases can be realized and that it shares many of the advantages of the two-dimensional scheme devised in [4], including numerical stability, accuracy, and efficiency.

The outline of the paper is as follows: In Section 2 we briefly recall the governing equations for the scattering of time-harmonic acoustic radiation from a three-dimensional obstacle. In Section 3 we discuss two boundary perturbation methods for acoustic scattering: "field expansions" (FE) and "transformed field expansions" (TFE). In Section 3.1 we recall the classical FE recursions [6] and present a numerical simulation which exhibits the algorithm's rather unstable nature. In Sections 3.2 and 3.3 we introduce the TFE method for addressing the scalar Helmholtz equation in three-dimensions, and in Section 4 we discuss the numerical implementation of the resulting TFE recursions. We conclude with numerical results presented in Section 5 which include comparisons with not only a family of exact solutions, but also highly resolved simulations of plane-wave configurations.

2. Governing equations

If time-harmonic plane-wave acoustic radiation of the form

$$v_i = e^{ik\alpha \cdot x}, \quad |\alpha| = 1, \tag{1}$$

is incident upon an obstacle Σ

$$\Sigma := \{(r, \theta, \phi) | 0 \leqslant r < a + g(\theta, \phi), 0 \leqslant \theta < 2\pi, 0 \leqslant \phi < \pi\},$$

then the (reduced) scattered field $v = v(r, \theta, \phi)$ is known to satisfy the scalar Helmholtz equation [1]

$$\Delta v + k^2 v = 0 \quad (r, \theta, \phi) \in \Omega, \tag{2}$$

where

$$\Omega := \{(r, \theta, \phi) | r > a + g(\theta, \phi), 0 \leqslant \theta < 2\pi, 0 \leqslant \phi < \pi\}.$$

Of course, to realize a unique solution one must specify, in addition to the periodicity in θ and ϕ, boundary conditions at the scatterer and at infinity. For the former, we choose a pressure release (sound-soft) condition which gives the following Dirichlet condition

$$v(a + g(\theta, \phi), \theta, \phi) = -v_i(a + g(\theta, \phi), \theta, \phi) =: \xi(\theta, \phi), \tag{3}$$

and defines the generic Dirichlet data ξ. We emphasize that a Neumann (sound-hard) boundary condition can be treated in a similar fashion. Regarding the behavior of solutions at infinity we have the Sommerfeld radiation condition:

$$\lim_{r \to \infty} r(\partial_r v - ikv) = 0. \tag{4}$$

Gathering (2)–(4) we have the well-known equations governing the scattering of time-harmonic, acoustic plane-waves from an irregular obstacle

$$\Delta v + k^2 v = 0 \quad (r, \theta, \phi) \in \Omega, \tag{5a}$$
$$v(a + g(\theta, \phi), \theta, \phi) = \xi(\theta, \phi), \tag{5b}$$
$$\lim_{r \to \infty} r(\partial_r v - ikv) = 0. \tag{5c}$$

2.1. A transparent boundary condition

One of the severe difficulties associated with the numerical simulation of the system (5) is the unbounded nature of the computational domain, Ω. In volumetric discretizations, such as the one we advocate here, this problem is usually addressed with the introduction of an "artificial boundary," and the imposition there of some boundary conditions motivated by the Sommerfeld radiation condition (4). We now describe a "transparent" or "exact" boundary condition which can be enforced on such an artificial boundary. For this, consider any $b > a + |g|_{L^\infty}$, giving rise to an artificial boundary at $r = b$, and the augmented scattering problem

$$\Delta v + k^2 v = 0 \quad (r, \theta, \phi) \in \Omega_{a+g,b}, \tag{6a}$$
$$v(a + g(\theta, \phi), \theta, \phi) = \xi(\theta, \phi), \tag{6b}$$
$$\partial_r v(b, \theta, \phi) = \partial_r w(b, \theta, \phi), \tag{6c}$$
$$v(b, \theta, \phi) = w(b, \theta, \phi), \tag{6d}$$
$$\Delta w + k^2 w = 0, \quad r > b, \tag{6e}$$
$$\lim_{r \to \infty} r(\partial_r w - ikw) = 0, \tag{6f}$$

where

$$\Omega_{r_1, r_2} := \{(r, \theta, \phi) | r_1 < r < r_2, 0 \leqslant \theta < 2\pi, 0 \leqslant \phi < \pi\}.$$

The solutions of (5) and (6) are identical in that the v match on $\Omega_{a+g,b}$, and $v = w$ on $r > b$. To specify the exact boundary condition on v at $r = b$ consider (6d)–(6f):

$$\Delta w + k^2 w = 0, \quad r > b, \tag{7a}$$
$$w(b, \theta, \phi) = \psi(\theta, \phi), \tag{7b}$$
$$\lim_{r \to \infty} r(\partial_r w - ikw) = 0, \tag{7c}$$

where ψ is meant to denote generic Dirichlet data at $r = b$. The exact solution of this system can be expressed as:

$$w(r, \theta, \phi) = \sum_{l=0}^{\infty} \sum_{m=-l}^{l} \hat{\psi}_{l,m} \left(\frac{r^{-1/2} H_{l+1/2}^{(1)}(kr)}{b^{-1/2} H_{l+1/2}^{(1)}(kb)} \right) Y_{l,m}(\theta, \phi),$$

where $H_{l+1/2}^{(1)}$ is the $(l + 1/2)$th Hankel function of the first kind, $Y_{l,m}$ is the spherical harmonic with index (l, m), and

$$\psi(\theta, \phi) = \sum_{l=0}^{\infty} \sum_{m=-l}^{l} \hat{\psi}_{l,m} Y_{l,m}(\theta, \phi).$$

We note here that $H_{l+1/2}^{(1)}$ is also known as $h_l^{(1)}$, the lth spherical Hankel function of the first kind. To satisfy (6c), given $\psi = w|_{r=b}$, we need to produce $\partial_r w|_{r=b}$, i.e. the Dirichlet–Neumann operator (DNO). More precisely, we define this DNO, T, by:

$$T[\psi] := \partial_r w(b, \theta, \phi) = \sum_{l=0}^{\infty} \sum_{m=-l}^{l} \hat{\psi}_{l,m} \left(k \frac{d_z H_{l+1/2}^{(1)}(kb)}{H_{l+1/2}^{(1)}(kb)} - \frac{1}{2b} \right) Y_{l,m}(\theta, \phi), \tag{8}$$

where

$$d_z H_{l+1/2}^{(1)}(kb) := \left. \frac{dH_{l+1/2}^{(1)}(z)}{dz} \right|_{z=kb}.$$

Therefore, based upon the augmented system (6), we can equivalently restate (5) on the *bounded* domain $\Omega_{a+g,b}$

$$\Delta v + k^2 v = 0 \quad (r, \theta, \phi) \in \Omega_{a+g,b}, \tag{9a}$$

$$v(a + g(\theta, \phi), \theta, \phi) = \xi(\theta, \phi), \tag{9b}$$

$$\partial_r v(b, \theta) - T[v(b, \theta)] = 0, \tag{9c}$$

with the transparent boundary condition at $r = b$ specified via the non-local DNO, T.

3. Boundary perturbation methods

Among the wide array of algorithms available for the numerical solution of bounded-obstacle scattering problems (see, e.g. [1–3]), a compelling choice for many configurations is based upon geometric perturbations of the boundary. First explored in their low-order incarnations by Rayleigh [7] and Rice [8], the high-order generalization (termed the "method of variation of boundaries") was fully explored in a series of papers by Bruno and Reitich [9–12,6,13]. In Section 3.1 we recall this algorithm (which has subsequently been renamed the method of "field expansions" (FE) [14–16]) and point out the inherent instability present in this method due to subtle cancellations in its recursions. It has been shown, however, that a slight modification of this procedure delivers an accurate and *stable* numerical approach which can be applied to quite general geometries [14,17,18,15,16,4]. This method of "transformed field expansions" (TFE) is now fully described for acoustic scattering in three-dimensional geometries in Section 3.3, and followed by numerical experiments which substantiate our claims of stability and high-order accuracy.

3.1. Field expansions and cancellations

If the shape of the scattering obstacle Σ can be viewed as a *small* perturbation of a separable geometry (e.g. a circle or ellipse) then a numerical perturbation method is not only natural but should also be highly accurate. This is the point of view taken in the derivation of the method of "field expansions" (FE) for the solution of the scattering problem (9) [7–12,6,13]. In particular, if we suppose that $g(\theta, \phi) = \varepsilon f(\theta, \phi)$ then it seems reasonable (and can be rigorously justified [19]) that

$$v(r, \theta, \phi; \varepsilon) = \sum_{n=0}^{\infty} v_n(r, \theta, \phi) \varepsilon^n,$$

where, from (9), the v_n must satisfy

$$\Delta v_n + k^2 v_n = 0 \quad (r, \theta, \phi) \in \Omega_{a,b}, \tag{10a}$$

$$v_n(a, \theta, \phi) = \delta_{n,0} \xi(\theta, \phi) - \sum_{j=0}^{n-1} \frac{f^{n-j}}{(n-j)!} \partial_r^{n-j} v_j(a, \theta, \phi), \tag{10b}$$

$$\partial_r v_n(b, \theta) - T[v_n(b, \theta)] = 0, \tag{10c}$$

cf. [6,19], and $\delta_{n,m}$ is the Kronecker delta. As we saw in Section 2.1, the exact solution of (10a) and (10c) can be written as

$$v_n(r, \theta, \phi) = \sum_{l=0}^{\infty} \sum_{m=-l}^{l} d_{n,l,m} \tilde{H}_l(r) Y_{l,m}(\theta, \phi),$$

where

$$\tilde{H}_l(r) := \frac{r^{-1/2} H_{l+1/2}^{(1)}(kr)}{a^{-1/2} H_{l+1/2}^{(1)}(ka)}.$$

To find the $d_{n,l,m}$ we appeal to (10b) which mandates that

$$\sum_{l=0}^{\infty} \sum_{m=-l}^{l} d_{n,l,m} Y_{l,m}(\theta,\phi) = \delta_{n,0} \sum_{l=0}^{\infty} \sum_{m=-l}^{l} \hat{\tilde{\xi}}_{l,m} Y_{l,m}(\theta,\phi) - \sum_{j=0}^{n-1} \left(\sum_{l=0}^{\infty} \sum_{m=-l}^{l} F_{n-j,l,m} Y_{l,m}(\theta,\phi) \right)$$
$$\times \left(\sum_{l=0}^{\infty} \sum_{m=-l}^{l} k^{n-j} d_z^{n-j} \tilde{H}_l(ka) Y_{l,m}(\theta,\phi) d_{j,l,m} \right), \tag{11}$$

where

$$F_j(\theta,\phi) := \frac{f^j(\theta,\phi)}{j!}, \quad F_j = \sum_{l=0}^{\infty} \sum_{m=-l}^{l} F_{j,l,m} Y_{l,m}(\theta,\phi).$$

This recursion, (11), can be written more simply as

$$d_{n,l,m} = \delta_{n,0} \hat{\tilde{\xi}}_{l,m} - \sum_{j=0}^{n-1} (F_{n-j} * A_{n,j})_{l,m}, \tag{12}$$

where

$$A_{n,j}(\theta,\phi) := \sum_{l=0}^{\infty} \sum_{m=-l}^{l} k^{n-j} d_z^{n-j} \tilde{H}_l(ka) Y_{l,m}(\theta,\phi) d_{j,l,m}$$

and $*$ denotes convolution. We point out that if all perturbation orders n and spherical harmonic coefficients (l,m) are retained then (12) gives an *exact* formula for the scattered field so, at this point, there is no approximation. Of course this is not possible in a numerical simulation, so both the perturbation order and spherical harmonic expansion are truncated after a finite number of terms, say N and (N_θ, N_ϕ), respectively. Note that, from the form of the spherical harmonic expansion, N_ϕ is not a free parameter as it depends linearly upon N_θ. Now, the only consideration left for an implementation is the resolution of the convolution; this can be achieved by the "spherical harmonic transform" (SHT) which, like the discrete Fourier transform (DFT), can be accelerated, e.g. [20].

Within their domain of applicability these FE recursions, (12), can provide highly (spectrally) accurate simulations of the scattered field in a very rapid fashion [6]. In fact, the total computational effort can be given by

$$\mathcal{O}(NF(N_\theta)),$$

where F is the complexity of the SHT that Suda and Takami [20] show can be $\mathcal{O}(N_\theta^2 \log(N_\theta))$. However, it was discovered by Nicholls and Reitich [14,17,18] that these recursions feature subtle but significant *cancellations* characterized by differences of very large numbers which are required to produce small numbers. This, of course, is a recipe for disaster in a finite precision numerical simulation.

To make this point clear we recall a calculation performed in our previous paper [4] which was conducted for a scatterer shaped by

$$\Sigma_{a,\varepsilon} := \{(r,\theta,z) | r < a + \varepsilon \cos(\theta)\},$$

(where $a = 1$ and $\varepsilon = 0.7$), i.e. a large but smooth deformation of a cylinder of infinite extent. In this test a numerical simulation of the normal derivative of the field at the surface of the scatterer (the current) using the FE method was compared with an exact solution. Also, a simulation of the current using our new method ("transformed field expansions" – TFE, see Section 3.3) was compared to the exact solution. The results of this experiment are summarized in Fig. 1 with measurements of L^∞ error versus perturbation order N. The numerical parameters are $N_\theta = 48$, $N_r = 48$, and $N = 23$, and the frequency is $k = 1$. We point out the striking divergence of the FE approximation from the exact solution beyond $N = 7$ in comparison with the TFE simulation which gives more accurate answers throughout all orders N. In particular, we note that the best answer that the FE method can ever deliver has L^∞ accuracy of 10^{-1} (when $N = 7$), while the TFE method gives answers reliable to 10^{-4} (at $N = 23$). As demonstrated in [17,15], while the *qualitative* features of Fig. 1 are quite
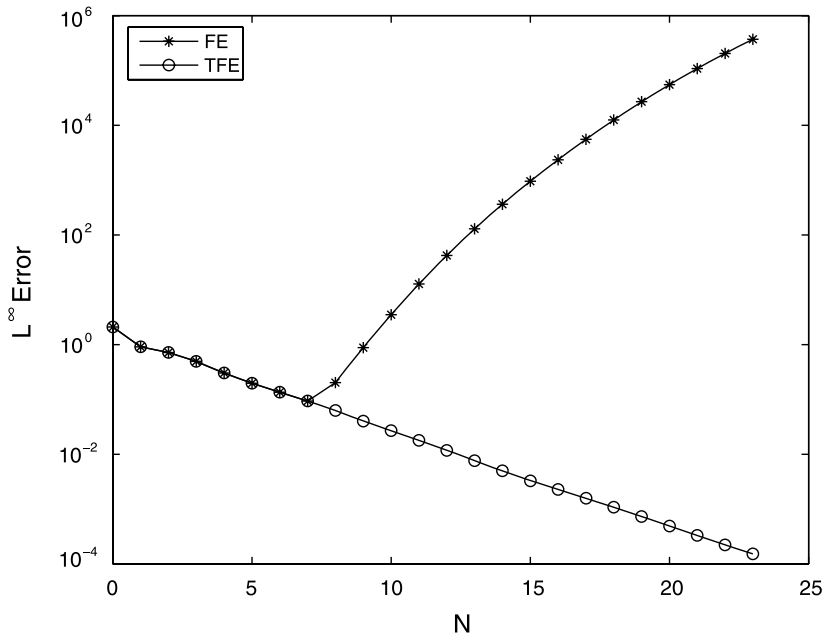
Fig. 1. L^∞-norm of difference between exact current and numerical approximations, versus perturbation order N. Both the FE (stars) and TFE (circles), see Section 3.3, approximations are plotted for the smooth perturbation $f(\theta) = \cos(\theta)$, $a = 1$, $\varepsilon = 0.7$, with parameters $N_\theta = 48$, $N_r = 48$, $N = 23$, $k = 1$. Notice the striking divergence of the FE approximation beyond $N = 7$ and the predictable, progressive convergence of the TFE approach throughout all orders.

generic, the *quantitative* details of the plot (e.g. divergence order of FE) can be manipulated by an astute choice of ε and f. We direct the interested reader to [14,17,18,15,16,21,4] (particularly [15]) for a complete discussion of these issues.

3.2. Change of variables

The TFE method, as applied to bounded-obstacle acoustic scattering in three dimensions, begins with the change of variables:

$$r' = \frac{(b-a)r - bg(\theta,\phi)}{(b-a) - g(\theta,\phi)} = \frac{dr - bg}{d - g}, \quad \theta' = \theta, \quad \phi' = \phi, \tag{13}$$

where $d := (b - a)$. This change of variables maps the complicated, perturbed geometry $\Omega_{a+g,b}$ to the simpler (separable) spherical shell $\Omega_{a,b}$. We now seek to restate (9) in these transformed coordinates for the transformed field

$$u(r',\theta',\phi') = v((r' + A(r',\theta',\phi'))/d, \theta', \phi'),$$

where A is defined in (14f). We start by listing some useful formulas for future reference:

$$(d - g(\theta,\phi))\partial_\theta = (d - g(\theta,\phi))\partial_{\theta'} - B(r',\theta',\phi')\partial_{r'}, \tag{14a}$$

$$(d - g(\theta,\phi))\partial_\phi = (d - g(\theta,\phi))\partial_{\phi'} - C(r',\theta',\phi')\partial_{r'}, \tag{14b}$$

$$(d - g(\theta,\phi))\partial_r = d\,\partial_{r'}, \tag{14c}$$

$$(d - g(\theta,\phi))D_\theta = (d - g)D_{\theta'} - F(r',\theta',\phi')\partial_{r'}, \tag{14d}$$

$$dr = d\,r' + A(r',\theta',\phi'). \tag{14e}$$

where $D_\theta := \sin(\theta)\partial_\theta$,

$$A(r', \theta', \phi') = g(\theta', \phi')(b - r'), \tag{14f}$$

$$B(r', \theta', \phi') = \partial_{\theta'} A = (\partial_{\theta'} g(\theta', \phi'))(b - r'), \tag{14g}$$

$$C(r', \theta', \phi') = \partial_{\phi'} A = (\partial_{\phi'} g(\theta', \phi'))(b - r'), \tag{14h}$$

$$F(r', \theta', \phi') = B \sin(\theta') = \sin(\theta')(\partial_{\theta'} g(\theta', \phi'))(b - r'). \tag{14i}$$

To begin the transformation of (9) we start with the Helmholtz equation (9a) in spherical coordinates:

$$0 = \partial_r(r^2 \partial_r v) + \frac{1}{\sin(\theta)} \partial_\theta(\sin(\theta) \partial_\theta v) + \frac{1}{\sin^2(\theta)} \partial_\phi^2 v + r^2 k^2 v.$$

Multiplying both sides by $(d - g)^2$ we obtain:

$$0 = (d - g)^2 \partial_r(r^2 \partial_r v) + (d - g)^2 \frac{1}{\sin(\theta)} \partial_\theta(\sin(\theta) \partial_\theta v) + (d - g)^2 \frac{1}{\sin^2(\theta)} \partial_\phi^2 v + (d - g)^2 r^2 k^2 v$$

$$=: V_1 + V_2 + V_3 + V_4.$$

We now address each of these terms separately:

$$V_1 = (d - g)^2 \partial_r(r^2 \partial_r v) = (d - g) \partial_r(r^2 d \partial_{r'} u) = \frac{d - g}{d} \partial_r[(dr' + A)^2 \partial_{r'} u] = \partial_{r'}[(dr' + A)^2 \partial_{r'} u]$$

$$= d^2 \partial_{r'}(r'^2 \partial_{r'} u) + 2d \partial_{r'}(r' A \partial_{r'} u) + \partial_{r'}[A^2 \partial_{r'} u],$$

and

$$V_2 = (d - g)^2 r^2 k^2 v = (d - g)^2 \left(r' + \frac{A}{d}\right)^2 k^2 u = (d^2 - 2dg + g^2)\left((r')^2 + \frac{2r'A}{d} + \frac{A^2}{d^2}\right) k^2 u$$

$$= d^2 (r')^2 k^2 u + \sum_{j=1}^{4} H_j(g) k^2 u,$$

where

$$H_1(g) := -2dg(r')^2 + 2dAr',$$

$$H_2(g) := g^2(r')^2 - 4gAr' + A^2,$$

$$H_3(g) := (2/d)Ag^2 r' - (2/d)gA^2,$$

$$H_4(g) := (1/d^2)g^2 A^2.$$

Next,

$$V_3 = \frac{1}{\sin(\theta)}(d - g)^2 \partial_\theta(\sin(\theta) \partial_\theta v) = \frac{1}{\sin(\theta)}(d - g)^2 \partial_\theta(D_\theta v)$$

$$= \frac{1}{\sin(\theta)}[(d - g)\partial_\theta((d - g)D_\theta)v + (\partial_\theta g)(d - g)D_\theta v]$$

$$= \frac{1}{\sin(\theta)}[((d - g)\partial_{\theta'} - B\partial_{r'})((d - g)D_{\theta'} - F\partial_{r'})u + (\partial_\theta g)((d - g)D_{\theta'} - F\partial_{r'})u]$$

$$= \frac{1}{\sin(\theta)}[(d - g)^2 \partial_{\theta'} D_{\theta'} u - (d - g)(\partial_{\theta'} g)D_{\theta'} u - (d - g)\partial_{\theta'}(F\partial_{r'} u) - (d - g)B\partial_{r'} D_{\theta'} u + B\partial_{r'}(F\partial_{r'} u)$$

$$+ (d - g)(\partial_{\theta'} g)D_{\theta'} u - (\partial_{\theta'} g)F\partial_{r'} u],$$

and

$$V_4 = \frac{1}{\sin^2(\theta)}(d-g)^2\partial_\phi^2 v = \frac{1}{\sin^2(\theta)}[((d-g)\partial_\phi)((d-g)\partial_\phi)v + (\partial_\phi g)(d-g)\partial_\phi v]$$

$$= \frac{1}{\sin^2(\theta)}[((d-g)\partial_{\phi'} - C\partial_{r'})((d-g)\partial_{\phi'} - C\partial_{r'})u + (\partial_{\phi'}g)((d-g)\partial_{\phi'} - C\partial_{r'})u]$$

$$= \frac{1}{\sin^2(\theta)}[(d-g)^2\partial_{\phi'}^2 u - (d-g)(\partial_{\phi'}g)\partial_{\phi'}u - (d-g)\partial_{\phi'}(C\partial_{r'}u) - (d-g)C\partial_{r'}\partial_{\phi'}u$$

$$+ C\partial_{r'}(C\partial_{r'}u) + (d-g)(\partial_{\phi'}g)\partial_{\phi'}u - (\partial_{\phi'}g)C\partial_{\phi'}u].$$

Despite their imposing forms, each of these terms can be significantly simplified using appropriate notation and several crucial identities. In this regard we define the operator:

$$\mathscr{I}[w] := \frac{1}{\sin(\theta)}\partial_\theta(\sin(\theta)\partial_\theta w) + \frac{1}{\sin^2(\theta)}\partial_\phi^2 w,$$

which is in fact the Laplace–Beltrami operator on the sphere and whose eigenfunctions are the spherical harmonics:

$$\mathscr{I}[Y_{l,m}] = \frac{1}{\sin(\theta)}\partial_\theta(\sin(\theta)\partial_\theta Y_{l,m}) + \frac{1}{\sin^2(\theta)}\partial_\phi^2 Y_{l,m} = -l(l+1)Y_{l,m}. \tag{15}$$

Furthermore, for any $h = h(r, \theta, \phi)$:

$$\partial_\phi(h\partial_\phi h) = (\partial_\phi h)^2 + h\partial_\phi^2 h,$$

$$\partial_\theta(\sin(\theta)h\partial_\theta h) = \sin(\theta)(\partial_\theta h)^2 + h\partial_\theta(\sin(\theta)\partial_\theta h),$$

so that

$$(\partial_\phi h)^2 = \partial_\phi(h\partial_\phi h) - h\partial_\phi^2 h,$$

$$(\partial_\theta h)^2 = \frac{1}{\sin(\theta)}\partial_\theta(\sin(\theta)h\partial_\theta h) - \frac{1}{\sin(\theta)}h\partial_\theta(\sin(\theta)\partial_\theta h).$$

From this we obtain

$$T_1 := \frac{1}{\sin^2(\theta)}(\partial_\phi h)^2 + (\partial_\theta h)^2$$

$$= \frac{1}{\sin^2(\theta)}\partial_\phi(h\partial_\phi h) - \frac{1}{\sin^2(\theta)}h\partial_\phi^2 h + \frac{1}{\sin(\theta)}\partial_\theta(\sin(\theta)h\partial_\theta h) - \frac{1}{\sin(\theta)}h\partial_\theta(\sin(\theta)\partial_\theta h)$$

$$= \left\{\frac{1}{\sin(\theta)}\partial_\theta(\sin(\theta)h\partial_\theta h) + \frac{1}{\sin^2(\theta)}\partial_\phi(h\partial_\phi h)\right\} - \left\{\frac{1}{\sin(\theta)}h\partial_\theta(\sin(\theta)\partial_\theta h) + \frac{1}{\sin^2(\theta)}h\partial_\phi^2 h\right\}$$

$$= \left\{\frac{1}{\sin(\theta)}\partial_\theta\left[\sin(\theta)\partial_\theta\left(\frac{1}{2}h^2\right)\right] + \frac{1}{\sin^2(\theta)}\partial_\phi\left[\partial_\phi\left(\frac{1}{2}h^2\right)\right]\right\} - h\left\{\frac{1}{\sin(\theta)}\partial_\theta(\sin\theta\partial_\theta h) + \frac{1}{\sin^2(\theta)}\partial_\phi^2 h\right\}$$

$$= \mathscr{I}\left[\frac{1}{2}h^2\right] - h\mathscr{I}[h].$$

Additionally, for any w and h, the following is true:

$$(\partial_\phi(w-h))^2 = (\partial_\phi w - \partial_\phi h)(\partial_\phi w - \partial_\phi h) = (\partial_\phi w)^2 + (\partial_\phi h)^2 - 2(\partial_\phi w)(\partial_\phi h),$$

so that

$$(\partial_\phi w)(\partial_\phi h) = \frac{1}{2}((\partial_\phi w)^2 + (\partial_\phi h)^2 - (\partial_\phi(w-h))^2).$$

Similarly,

$$(\partial_\theta w)(\partial_\theta h) = \frac{1}{2}((\partial_\theta w)^2 + (\partial_\theta h)^2 - (\partial_\theta (w-h))^2).$$

Consequently, using the linearity of $\mathscr{I}$,

$$
\begin{aligned}
T_2 :&= \frac{1}{\sin^2(\theta)}(\partial_\phi w)(\partial_\phi h) + (\partial_\theta w)(\partial_\theta h) \\
&= \frac{1}{2}\left\{ \frac{1}{\sin^2(\theta)}(\partial_\phi w)^2 + \frac{1}{\sin^2(\theta)}(\partial_\phi h)^2 - \frac{1}{\sin^2(\theta)}(\partial_\phi(w-h))^2 + (\partial_\theta w)^2 + (\partial_\theta h)^2 - (\partial_\theta(w-h))^2 \right\} \\
&= \frac{1}{2}\left\{ \left(\frac{1}{\sin^2(\theta)}(\partial_\phi w)^2 + (\partial_\theta w)^2 \right) + \left(\frac{1}{\sin^2(\theta)}(\partial_\phi h)^2 + (\partial_\theta h)^2 \right) - \left(\frac{1}{\sin^2(\theta)}(\partial_\phi(w-h))^2 + (\partial_\theta(w-h))^2 \right) \right\} \\
&= \frac{1}{2}\left\{ \mathscr{I}\left[\frac{1}{2}w^2\right] - w\mathscr{I}[w] + \mathscr{I}\left[\frac{1}{2}h^2\right] - h\mathscr{I}[h] - \mathscr{I}\left[\frac{1}{2}(w-h)^2\right] + (w-h)\mathscr{I}[w-h] \right\} \\
&= \frac{1}{2}\{\mathscr{I}[wh] - h\mathscr{I}[w] - w\mathscr{I}[h]\}.
\end{aligned}
$$

We can also show that

$$\partial_{\phi'}(C\partial_{r'}u) = C\partial_{r'}\partial_{\phi'}u + (\partial_{r'}u)(\partial_{\phi'}C) = C\partial_{r'}\partial_{\phi'}u + (\partial_{r'}u)(\partial_{\phi'}^2 g)(b-r'), \tag{16}$$

and, similarly,

$$\partial_{\theta'}(F\partial_{r'}u) = \partial_{\theta'}((D_{\theta'}g)(b-r')\partial_{r'}u) = (\partial_{\theta'}D_{\theta'}g)(b-r')\partial_{r'}u + (D_{\theta'}g)((b-r')\partial_{\theta'}\partial_{r'}u). \tag{17}$$

We are now in a position to simplify the following radial contribution to the Laplacian:

$$I := \frac{1}{\sin(\theta)}(d-g)^2\partial_\theta(\sin(\theta)\partial_\theta v) + \frac{1}{\sin^2(\theta)}(d-g)^2\partial_\phi^2 v.$$

Applying the change variables (13), we find:

$$
\begin{aligned}
I =\ & \frac{1}{\sin(\theta)}\{(d-g)^2\partial_{\theta'}D_{\theta'}u - (d-g)(\partial_{\theta'}g)D_{\theta'}u - (d-g)\partial_{\theta'}(F\partial_{r'}u) - (d-g)B\partial_{r'}D_{\theta'}u + B\partial_{r'}(F\partial_{r'}u) \\
& + (d-g)(\partial_{\theta'}g)D_{\theta'}u - (\partial_{\theta'}g)F\partial_{r'}u\} + \frac{1}{\sin^2(\theta)}\{(d-g)^2\partial_{\phi'}^2 u - (d-g)(\partial_{\phi'}g)\partial_{\phi'}u - (d-g)\partial_{\phi'}(C\partial_{r'}u) \\
& - (d-g)C\partial_{r'}\partial_{\phi'}u + C\partial_{r'}(C\partial_{r'}u) + (d-g)(\partial_{\phi'}g)\partial_{\phi'}u - (\partial_{\phi'}g)C\partial_{\phi'}u\}.
\end{aligned}
$$

Using (16) and (17):

$$
\begin{aligned}
I =\ & (d-g)^2\left(\frac{1}{\sin^2(\theta)}\partial_{\phi'}^2 u + \frac{1}{\sin(\theta)}\partial_{\theta'}D_{\theta'}u \right) + \frac{2}{\sin^2(\theta)}C(g-d)\partial_{r'}\partial_{\phi'}u + \frac{1}{\sin^2(\theta)}(g-d)(b-r')\partial_{r'}u(\partial_{\phi'}^2 g) \\
& - \frac{2}{\sin^2(\theta)}C\partial_{\phi'}g\partial_{r'}u + \frac{1}{\sin(\theta)}(g-d)(b-r')\partial_{r'}u(\partial_{\theta'}D_{\theta'}g) + \frac{1}{\sin(\theta)}(g-d)(D_{\theta'}g)(b-r')\partial_{\theta'}\partial_{r'}u \\
& - 2\frac{1}{\sin(\theta)}(D_{\theta'}g)(\partial_{r'}u)B + \frac{1}{\sin(\theta)}(g-d)B\partial_{r'}D_{\theta'}u + \frac{1}{\sin^2(\theta)}C(b-r')(\partial_{\phi'}g)\partial_{r'}^2 u + \frac{1}{\sin(\theta)}B(D_{\theta'}g)(b-r')\partial_{r'}^2 u,
\end{aligned}
$$

and, after rearranging terms, we obtain

$$
\begin{aligned}
I &= \left\{ (d-g)^2 \left(\frac{1}{\sin^2(\theta)} \partial_{\phi'}^2 u + \frac{1}{\sin(\theta)} \partial_{\theta'} D_{\theta'} u \right) \right\} \\
&\quad + \left\{ \frac{2}{\sin^2(\theta)} C(g-d)\partial_{r'}\partial_{\phi'}u + \frac{1}{\sin(\theta)}(g-d)(D_{\theta'}g)(b-r')\partial_{\theta'}\partial_{r'}u + \frac{1}{\sin(\theta)}(g-d)B\partial_{r'}D_{\theta'}u \right\} \\
&\quad + \left\{ \frac{1}{\sin^2(\theta)}(g-d)(b-r')\partial_{r'}u(\partial_{\phi'}^2 g) + \frac{1}{\sin(\theta)}(g-d)(b-r')\partial_{r'}u(\partial_{\theta'}D_{\theta'}g) \right\} \\
&\quad - 2\left\{ \frac{1}{\sin^2(\theta)} C(\partial_{\phi'}g)\partial_{r'}u + \frac{1}{\sin(\theta)}(D_{\theta'}g)(\partial_{r'}u)B \right\} \\
&\quad + \left\{ \frac{1}{\sin^2(\theta)} C(b-r')(\partial_{\phi'}g)\partial_{r'}^2 u + \frac{1}{\sin(\theta)} B(D_{\theta'}g)(b-r')\partial_{r'}^2 u \right\}.
\end{aligned}
$$

Simplifying further

$$
\begin{aligned}
I &= \left\{ (d-g)^2 \left(\frac{1}{\sin^2(\theta)} \partial_{\phi'}^2 u + \frac{1}{\sin(\theta)} \partial_{\theta'} D_{\theta'} u \right) \right\} \\
&\quad + 2\left\{ (g-d)(b-r') \left(\frac{1}{\sin^2(\theta)}(\partial_{\phi'}g)\partial_{\phi'}(\partial_{r'}u) + (\partial_{\theta'}g)\partial_{\theta'}(\partial_{r'}u) \right) \right\} \\
&\quad + (g-d)(b-r')\partial_{r'}u \left\{ \frac{1}{\sin^2(\theta)}(\partial_{\phi'}^2 g) + \frac{1}{\sin(\theta)}\partial_{\theta'}(\sin(\theta)(\partial_{\theta'}g)) \right\} \\
&\quad - 2(b-r')\partial_{r'}u \left\{ \frac{1}{\sin^2(\theta)}(\partial_{\phi'}g)^2 + (\partial_{\theta'}g)^2 \right\} + (b-r')^2\partial_{r'}^2 u \left\{ \frac{1}{\sin^2(\theta)}(\partial_{\phi'}g)^2 + (\partial_{\theta'}g)^2 \right\},
\end{aligned}
$$

and using (15) we find:

$$
\begin{aligned}
I &= (d-g)^2 \mathscr{I}[u] + (g-d)(b-r')\{\mathscr{I}[g\partial_{r'}u] - g\mathscr{I}[\partial_{r'}u] - (\mathscr{I}[g])\partial_{r'}u\} \\
&\quad + (g-d)(b-r')\partial_{r'}u\mathscr{I}[g] - 2(b-r')\partial_{r'}u\left\{ \mathscr{I}\left[\frac{1}{2}g^2\right] - g\mathscr{I}[g] \right\} \\
&\quad + (b-r')^2\partial_{r'}^2 u\left\{ \mathscr{I}\left[\frac{1}{2}g^2\right] - g\mathscr{I}[g] \right\}, \\
&= d^2\mathscr{I}[u] - 2dg\mathscr{I}[u] + g^2\mathscr{I}[u] - d(\mathscr{I}[g])(b-r')\partial_{r'}u + (b-r')g(\mathscr{I}[g])\partial_{r'}u \\
&\quad - 2\left\{ \mathscr{I}\left[\frac{1}{2}g^2\right] - g\mathscr{I}[g] \right\}(b-r')\partial_{r'}u + \left\{ \mathscr{I}\left[\frac{1}{2}g^2\right] - g\mathscr{I}[g] \right\}(b-r')^2\partial_{r'}^2 u \\
&\quad - d(b-r')\mathscr{I}[g\partial_{r'}u] + g(b-r')\mathscr{I}[g\partial_{r'}u] + d(b-r')g\mathscr{I}[\partial_{r'}u] \\
&\quad - g^2(b-r')\mathscr{I}[\partial_{r'}u] + d(b-r')(\mathscr{I}[g])\partial_{r'}u - g(b-r')(\mathscr{I}[g])\partial_{r'}u.
\end{aligned}
$$

Finally, the original Helmholtz equation (9a) becomes

$$
\partial_{r'}(r'\partial_{r'}u) + \mathscr{I}[u] + (r')^2 k^2 u = F(r',\theta',\phi';u)
$$

where

$$
\begin{aligned}
-d^2 F &= 2d\partial_{r'}(r'A\partial_{r'}u) + \partial_{r'}(A^2\partial_{r'}u) - 2dg\mathscr{I}[u] + g^2\mathscr{I}[u] - d\mathscr{I}[g](b-r')\partial_{r'}u + (b-r')g\mathscr{I}[g]\partial_{r'}u \\
&\quad - 2\left\{ \mathscr{I}\left[\frac{1}{2}g^2\right] - g\mathscr{I}[g] \right\}(b-r')\partial_{r'}u + \left\{ \mathscr{I}\left[\frac{1}{2}g^2\right] - g\mathscr{I}[g] \right\}(b-r')^2\partial_{r'}^2 u - d(b-r')\mathscr{I}[g\partial_{r'}u] + g(b-r')\mathscr{I}[g\partial_{r'}u] \\
&\quad + d(b-r')g\mathscr{I}[\partial_{r'}u] - g^2(b-r')\mathscr{I}[\partial_{r'}u] + d(b-r')\mathscr{I}[g]\partial_{r'}u - g(b-r')\mathscr{I}[g]\partial_{r'}u + \sum_{j=1}^{4} H_j(g)k^2 u.
\end{aligned}
$$

The Dirichlet condition, (9b), simply transforms to

$$u(a, \theta', \phi') = \xi(\theta', \phi')$$

while (9c), upon multiplication by $(d - g)$, can be written as

$$0 = (d - g)\partial_r v(b, \theta, \phi) - (d - g)T[v(b, \theta, \phi)] = d\partial_{r'} u(b, \theta', \phi') - dT'[u(b, \theta', \phi')] + g\, T'[u(b, \theta', \phi')].$$

Since $T' = T$, (9c) transforms to

$$\partial_{r'} u(b, \theta', \phi') - T[u(b, \theta', \phi')] = J(\theta', \phi'),$$

where

$$dJ(\theta', \phi') = -gT[u(b, \theta', \phi')].$$

Collecting all of these transformed equations, we find that u, upon dropping primes, satisfies

$$\partial_r(r^2\partial_r u) + \mathscr{J}[u] + r^2 k^2 u = F(r, \theta, \phi; u, g) \quad (r, \theta, \phi) \in \Omega_{a,b}, \tag{18a}$$
$$u(a, \theta, \phi) = \xi(\theta, \phi), \tag{18b}$$
$$\partial_r u(b, \theta, \phi) - T[u(b, \theta, \phi)] = J(\theta, \phi; u, g). \tag{18c}$$

3.3. Transformed field expansions

Consider the transformed field u; setting $g = \varepsilon f$ it is possible, following the method of Nicholls and Reitich [14,18] and Nicholls and Nigam [19], to prove the following analyticity theorem.

Theorem 1. *Given an integer $s \geqslant 0$, if $f \in C^{s+2}$ and $\xi \in H^{s+3/2}$, there exists a unique solution*

$$u(r, \theta, \phi; \varepsilon) = \sum_{n=0}^{\infty} u_n(r, \theta, \phi)\varepsilon^n \tag{19}$$

of (18) satisfying, for some positive constants C and K,

$$\|u_n\|_{s+2} \leqslant K\|\xi\|_{s+3/2}B^n$$

for any $B > C|f|_{C^{s+2}}$.

Following [4], we insert the *strongly* convergent series (19) into (18) and derive recursions for the $\{u_n\}$:

$$\partial_r(r^2\partial_r u_n) + \mathscr{J}[u_n] + r^2 k^2 u_n = F_n(r, \theta, \phi) \quad (r, \theta, \phi) \in \Omega_{a,b}, \tag{20a}$$
$$u_n(a, \theta, \phi) = \delta_{n,0}\xi(\theta, \phi), \tag{20b}$$
$$\partial_r u_n(b, \theta, \phi) - T[u_n(b, \theta, \phi)] = J_n(\theta, \phi), \tag{20c}$$

where $\delta_{n,p}$ is the Kronecker delta,

$$\begin{aligned}
-d^2 F_n = {} & 2d\partial_r(rA\partial_r u_{n-1}) + \partial_r(A^2\partial_r u_{n-2}) - 2df\,\mathscr{J}[u_{n-1}] + f^2\mathscr{J}[u_{n-2}] - d\mathscr{J}[f](b-r)\partial_r u_{n-1} \\
& + (b-r)f\;\mathscr{J}[f]\partial_r u_{n-2} - 2\left\{\mathscr{J}\left[\frac{1}{2}f^2\right] - f\mathscr{J}[f]\right\}(b-r)\partial_r u_{n-2} \\
& + \left\{\mathscr{J}\left[\frac{1}{2}f^2\right] - f\mathscr{J}[f]\right\}(b-r)^2\partial_r^2 u_{n-2} - d(b-r)\mathscr{J}[f\partial_r u_{n-1}] + f(b-r)\mathscr{J}[f\partial_r u_{n-2}] \\
& + d(b-r)f\,\mathscr{J}[\partial_r u_{n-1}] - f^2(b-r)\mathscr{J}[\partial_r u_{n-2}] + d(b-r)\mathscr{J}[f]\partial_r u_{n-1} - f(b-r)\mathscr{J}[f]\partial_r u_{n-2} \\
& + \sum_{j=1}^{4} H_j(f)k^2 u_{n-j}, \tag{20d}
\end{aligned}$$

and

$$dJ_n = -fT[u_{n-1}(b, \theta, \phi)]. \tag{20e}$$

We emphasize that F_n only involves u_{n-j} $(j = 1, 2, 3, 4)$ and J_n only depends on u_{n-1}. Hence, for each n, u_n can be determined from (20) which is simply an inhomogeneous Helmholtz equation on a spherical shell with inhomogeneous data. In the next section we present an efficient spectral-Galerkin method for the numerical simulation of (20).

Remark 2. At this point we remark that our new TFE method can still be used, with minor modification, to treat the *inhomogeneous* problem of scattering in the presence of a (compactly supported) source near the obstacle. This can be accurately modeled with the addition of a "source" function $S(r, \theta, \phi)$ to the right-hand side of (2). It is not difficult to see that this S will propagate to the right-hand side of (18a) intact after the change of variables. However, in a completely "honest" implementation of the method one must consider that in the transformed coordinates this function S will depend upon g (and consequently ε) so that for each S considered, a Taylor expansion must be found and the nth order term, S_n, will appear on the right-hand side of (20a).

However, we can avoid this complication by careful consideration of the benefit of our method, i.e. that it produces *linear* (though recursive) problems for the *unknowns*, u_n. Fortunately, S is known for us so that upon transformation to the new coordinates we can "ignore" the implicit dependence upon g and simply view it as a new function $\tilde{S}$ depending solely on the transformed variables (r', θ', ϕ'). Now, when we expand in powers of ε, $\tilde{S}$ will only appear at order zero in (20a) and no Taylor series expansion is necessary. (Notice that if we attempt to ignore the implicit dependence of u upon ε then we must solve a *nonlinear* problem for u which is what we aim to avoid.) In this way we can easily incorporate general source functions S in our solution technique.

4. Spectral-Galerkin algorithm

Clearly, for the TFE method outlined above, (20), to be a competitive and reliable algorithm for the simulation of scattering configurations, we must devise a highly accurate and robust scheme for solving the Helmholtz equation (20a) coupled to the nonstandard boundary conditions (20b) and (20c). For this we advocate a spectral-Galerkin method based upon Legendre polynomials very much in the spirit of the method detailed in [4]. While the design philosophy of the two-dimensional method [4] is very similar to the one we outline below, we now provide, for the reader's convenience, a complete account of the algorithm.

As stated above, for each n, we need to find u_n by solving the following Helmholtz equation in a spherical shell:

$$\partial_r(r^2 \partial_r U) + \mathscr{J}[U] + r^2 k^2 U = F \quad (r, \theta, \phi) \in \Omega_{a,b}, \tag{21a}$$

$$U(a, \theta, \phi) = \xi(\theta, \phi), \tag{21b}$$

$$\partial_r U(b, \theta, \phi) - T[U(b, \theta, \phi)] = \eta(\theta, \phi), \tag{21c}$$

where $F(r, \theta, \phi)$, $\xi(\theta, \phi)$ and $\eta(\theta, \phi)$ are given functions. It is well known that the main difficulty in using the exact DNO, T, in the boundary condition at the artificial boundary is that it is a global operator. This leads to a dense sub-block in the linear system generated by a Galerkin method to solve (21) associated with (artificial) boundary unknowns. An important observation is that while this operator T is global in physical space, it is "local" in frequency space, see (8). To take advantage of this fact, we expand the solutions, $U(r, \theta, \phi)$, $F(r, \theta, \phi)$, $\xi(\theta, \phi)$, and $\eta(\theta, \phi)$, in spherical harmonic series

$$(U(r, \theta, \phi), F(r, \theta, \phi)) = \sum_{l=0}^{\infty} \sum_{m=-l}^{l} (\hat{u}_{l,m}(r), \hat{f}_{l,m}(r)) Y_{l,m}(\theta, \phi),$$

$$(\xi(\theta, \phi), \eta(\theta, \phi)) = \sum_{l=0}^{\infty} \sum_{m=-l}^{l} (\hat{\xi}_{l,m}, \hat{\eta}_{l,m}) Y_{l,m}(\theta, \phi).$$

Recalling the definition of the DNO, (8), it is easy to see that we can decompose (21) into the following sequence of one-dimensional, two-point boundary value problems:

$$\partial_r(r^2\partial_r\hat{u}_{l,m}) + (r^2k^2 - l(l+1))\hat{u}_{l,m} = \hat{f}_{l,m}, \quad r \in (a,b), \tag{22a}$$

$$\hat{u}_{l,m}(a) = \hat{\tilde{\xi}}_{l,m}, \tag{22b}$$

$$\partial_r\hat{u}_{l,m}(b) - \left(k\frac{d_zH^{(1)}_{l+1/2}(kb)}{H^{(1)}_{l+1/2}(kb)} - \frac{1}{2b}\right)\hat{u}_{l,m}(b) = \hat{\eta}_{l,m}. \tag{22c}$$

It is known from [22,23] that

$$\mathrm{Im}\left\{\frac{d_zH^{(1)}_{l+1/2}(kb)}{H^{(1)}_{l+1/2}(kb)}\right\} > 0, \quad \mathrm{Re}\left\{\frac{d_zH^{(1)}_{l+1/2}(kb)}{H^{(1)}_{l+1/2}(kb)}\right\} < 0, \quad -\frac{d_zH^{(1)}_{l+1/2}(kb)}{H^{(1)}_{l+1/2}(kb)} \sim \frac{l+1/2+1}{b} \quad \text{as } l \to \infty, \tag{23}$$

which implies the well-posedness of the problem (22).

To describe the spectral-Galerkin method for (22), let us first make a change of variables

$$x = \frac{2(r-a)}{b-a} - 1, \tag{24}$$

which maps $r \in (a,b)$ to $x \in I := (-1,1)$. If we denote

$$\tilde{u}_{l,m}(x) := \hat{u}_{l,m}(r), \quad \tilde{f}_{l,m}(x) := \hat{f}_{l,m}(r), \quad \tilde{\eta}_{l,m} := \hat{\eta}_{l,m}, \quad \tilde{\tilde{\xi}}_{l,m} := \hat{\tilde{\xi}}_{l,m},$$

$$c := \frac{b+a}{b-a}, \quad \omega := \frac{k(b-a)}{2}, \quad t_a := \frac{2}{b-a}, \quad t_b := -k\frac{d_zH^{(1)}_{l+1/2}(kb)}{H^{(1)}_{l+1/2}(kb)} + \frac{1}{2b},$$

then, (22) becomes:

$$\partial_x((x+c)^2\partial_x\tilde{u}_{l,m}) + ((x+c)^2\omega^2 - l(l+1))\tilde{u}_{l,m} = \tilde{f}_{l,m}, \quad x \in I, \tag{25a}$$

$$\tilde{u}_{l,m}(-1) = \tilde{\tilde{\xi}}_{l,m}, \tag{25b}$$

$$t_a\partial_x\tilde{u}_{l,m}(1) + t_b\tilde{u}_{l,m}(1) = \tilde{\eta}_{l,m}. \tag{25c}$$

It is straightforward to show that the functions

$$h_{l,m}(x) := \left(\frac{\tilde{\eta}_{l,m} - t_b\tilde{\tilde{\xi}}_{l,m}}{t_a + 2t_b}\right)x + \frac{\tilde{\eta}_{l,m} + t_b\tilde{\tilde{\xi}}_{l,m} + t_a\tilde{\tilde{\xi}}_{l,m}}{t_a + 2t_b}$$

satisfy the two boundary conditions in (25). Hence, setting

$$\delta := \frac{\tilde{\eta}_{l,m} - t_b\tilde{\tilde{\xi}}_{l,m}}{t_a + 2t_b}, \quad f_{l,m} := \tilde{f}_{l,m} - ((x+c)^2\omega^2 - l(l+1))h_{l,m} - 2\delta(x+c), \quad \tilde{u}_{l,m}(x) = u_{l,m}(x) + h_{l,m}(x),$$

we can rewrite (25) as the following problem with homogeneous boundary conditions:

$$\partial_x((x+c)^2\partial_x u_{l,m}) + ((x+c)^2\omega^2 - l(l+1))u_{l,m} = f_{l,m}, \quad x \in I, \tag{26a}$$

$$u_{l,m}(-1) = 0, \tag{26b}$$

$$t_a\partial_x u_{l,m}(1) + t_b u_{l,m}(1) = 0. \tag{26c}$$

To continue our specification, let us denote by P_N the space of complex-valued polynomials of degree less than or equal to N, and

$$X_N^{(l,m)} := \{u \in P_N | u(-1) = 0, t_a\partial_x u(1) + t_b u(1) = 0\}.$$

The spectral-Galerkin method for (26) is to find $u_N^{(l,m)} \in X_N^{(l,m)}$ such that

$$\int_I \partial_x((x+c)^2\partial_x u_N^{(l,m)})\bar{v}_N \, dx + \int_I ((x+c)^2\omega^2 - l(l+1))u_N^{(l,m)}\bar{v}_N \, dx = \int_I f_{l,m}\bar{v}_N \, dx, \quad \forall v_N \in X_N^{(l,m)}, \tag{27}$$

where $\bar{v}_N$ is the complex conjugate of v_N. We recall that if t_a and t_b are real numbers and P_N consists of real polynomials, then there exist unique real numbers $(\alpha_k^{(l,m)}, \beta_k^{(l,m)})$ such that

$$X_N^{(l,m)} = \text{span}\{\gamma_0^{(l,m)}(x), \gamma_1^{(l,m)}(x), \ldots, \gamma_{N-2}^{(l,m)}(x)\},$$

where

$$\gamma_k^{(l,m)}(x) = L_k(x) + \alpha_k^{(l,m)} L_{k+1}(x) + \beta_k^{(l,m)} L_{k+2}(x),$$

and $L_k(x)$ is the kth Legendre polynomial [24,25]. It is easy to see that this is still true if we allow all of the $(\alpha_k^{(l,m)}, \beta_k^{(l,m)})$, t_a, t_b, P_N, and $X_N^{(l,m)}$ to be complex valued. In fact, one easily verifies that

$$\alpha_k^{(l,m)} = \frac{(2k+3)t_a}{t_a(k+2)^2 + 2t_b}, \quad \beta_k^{(l,m)} = \alpha_k^{(l,m)} - 1.$$

We note that from (23), $\text{Re}\{t_b\} > 0$, so that $(\alpha_k^{(l,m)}, \beta_k^{(l,m)})$ are always well defined. Therefore, setting

$$u_N^{(l,m)}(x) := \sum_{j=0}^{N-2} u_j^{(l,m)} \gamma_j(x), \quad \mathbf{u}^{(l,m)} := (u_0^{(l,m)}, u_1^{(l,m)}, \ldots, u_{N-2}^{(l,m)})^{\mathrm{T}},$$

$$a_{j,n}^{(l,m)} := \int_I \partial_x((x+c)^2 \partial_x \gamma_n^{(l,m)}) \bar{\gamma}_j^{(l,m)} \, dx, \quad A^{(l,m)} := (a_{j,n}^{(l,m)}),$$

$$b_{j,n}^{(l,m)} := \int_I ((x+c)^2 \omega^2 - l(l+1)) \gamma_n^{(l,m)} \bar{\gamma}_j^{(l,m)} \, dx, \quad B^{(l,m)} := (b_{j,n}^{(l,m)}),$$

$$f_j^{(l,m)} := \int_I f_{l,m} \bar{\gamma}_j^{(l,m)} \, dx, \quad \mathbf{f}^{(l,m)} := (f_0^{(l,m)}, f_1^{(l,m)}, \ldots, f_{N-2}^{(l,m)})^{\mathrm{T}},$$

the system (27) becomes the following complex-valued system of equations:

$$(A^{(l,m)} + B^{(l,m)})\mathbf{u}^{(l,m)} = \mathbf{f}^{(l,m)}. \tag{28}$$

Due to the special form of $\gamma_j^{(l,m)}$, we additionally have that

$$b_{j,n}^{(l,m)} = 0, \quad |j-n| > 4, \quad a_{j,n}^{(l,m)} = 0, \quad n < j - 2.$$

Hence, for each l and m, the linear system (28) can be solved in $\mathcal{O}(N^2)$ operations by using a direct Gaussian elimination process. Renaming N as N_r, the spherical harmonic-Legendre approximation for (21) is given (with x defined by (24)) by:

$$U_{N_r,N_\theta}(r,\theta,\phi) = \sum_{l=0}^{N_\theta-1} \sum_{m=-l}^{l} \sum_{j=0}^{N_r-2} (u_j^{(l,m)} \gamma_j^{(l,m)}(x) + h_{l,m}(x)) Y_{l,m}(\theta,\phi) \tag{29}$$

which is the solution of the following approximate variational problem:

$$-(r^2 \partial_r U_{N_r,N_\theta}, \partial_r v) - \left(\sin(\theta) \partial_\theta U_{N_r,N_\theta}, \partial_\theta \left[\frac{1}{\sin(\theta)} v\right]\right)$$

$$-\left(\partial_\phi U_{N_r,N_\theta}, \partial_\phi \left[\frac{1}{\sin^2(\theta)} v\right]\right) + k^2(r^2 U_{N_r,N_\theta}, v) = (F, v) \quad \forall v \in V_{N_r,N_\theta},$$

$$U_{N_r,N_\theta}(a,\theta,\phi) = \xi_{N_\theta}(\theta,\phi),$$

$$\partial_r U_{N_r,N_\theta}(b,\theta,\phi) - T[U_{N_r,N_\theta}(b,\theta,\phi)] = \eta_{N_\theta}(\theta,\phi),$$

where $(\cdot,\cdot)$ is the L^2 inner product,

$$V_{N_r,N_\theta} = \text{span}\{\gamma_j^{(l,m)}(x(r)) Y_{lm}(\theta,\phi) | 0 \leqslant |m| \leqslant l \leqslant N_\theta - 1, 0 \leqslant j \leqslant N_r - 2\},$$

and,

$$(\xi_{N_\theta}(\theta,\phi), \eta_{N_\theta}(\theta,\phi)) = \sum_{l=0}^{N_\theta-1} \sum_{m=-l}^{l} (\hat{\xi}_{l,m}, \hat{\eta}_{l,m}) Y_{l,m}(\theta,\phi).$$

Having now completely specified our numerical algorithm we can comment on its computational complexity. As we have seen, in a simulation that retains N perturbation orders we must solve the equation (20) $(N+1)$-many times. Each of these problems is equivalent to the generic Helmholtz problem (21) which, in turn, amounts to a one-dimensional problem (22) for each pair (l, m). To convert (21) to (22) requires a spherical harmonic transform (SHT) at cost $\mathcal{O}(F(N_\theta))$. We have just seen that (22) can be solved in quadratic time in the discretization parameter N_r, thus the computational cost is:

$$\mathcal{O}(NF(N_\theta)N_r^2).$$

As we stated earlier, Suda and Takami [20] have shown that the SHT can be accomplished in time proportional to $\mathcal{O}(N_\theta^2 \log(N_\theta))$ so that the cost of our algorithm is:

$$\mathcal{O}(NN_\theta^2 \log(N_\theta)N_r^2).$$

Finally, we point out that the numerical analysis of this spectral-Galerkin approximation to (21) is performed in [26] which shows that the L^2-error decays exponentially fast as soon as N_r and N_θ are sufficiently large to resolve the wave in the spherical shell. We refer to [26] for a precise description of the error estimates. We also note that the error analysis for a related problem (where T in (21) is replaced by ik) was done in [27].

We now present numerical results demonstrating the spectral accuracy of the above scheme for the Helmholtz problem (21). For this we note that we have a family of *exact* solutions to the homogeneous Helmholtz equation, (21a), of the form:

$$U_{l,m}(r, \theta, \phi) := r^{-1/2} H_{l+1/2}^{(1)}(kr) Y_{l,m}(\theta, \phi). \tag{30}$$

Upon choosing (l, m) we can use this as an exact solution for the full problem, (21), provided that we set

$$F(r, \theta, \phi) = 0, \quad \xi(\theta, \phi) = a^{-1/2} H_{l+1/2}^{(1)}(ka) Y_{l,m}(\theta, \phi), \quad \eta(\theta, \phi) = 0. \tag{31}$$

To specify a particular numerical experiment, we now choose $a = 2$, $b = 4$, $l = 2$, and $m = 1$ and report, in Fig. 2, the results of using our spherical harmonic-Legendre algorithm. We observe that for any fixed k, the error converges exponentially as soon as enough modes are used to resolve the wave.
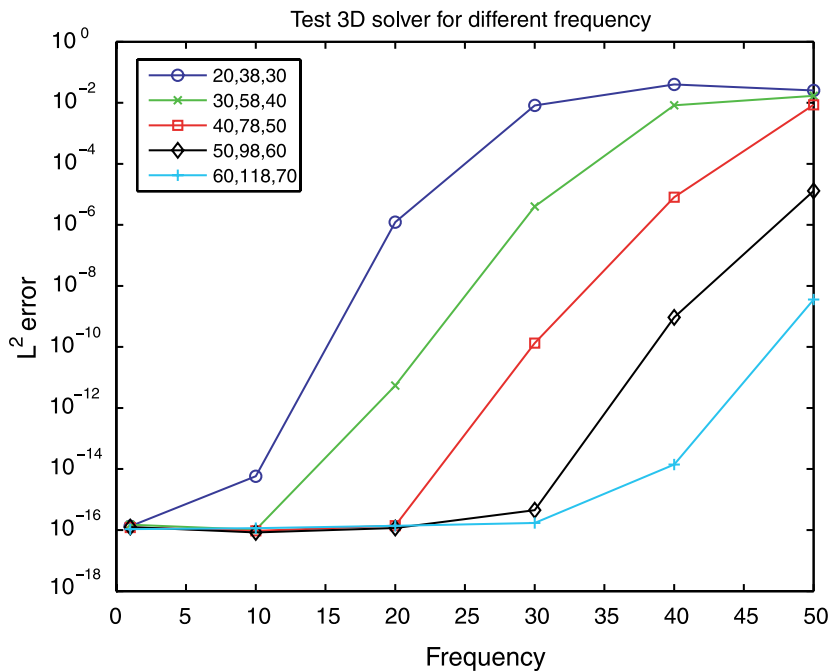

Fig. 2. Error, measured in L^2, between an exact solution, (30), of the Helmholtz equation, (22), and our spherical harmonic-Legendre approximation for different frequencies k. In the figure, the number triples denote the number of colatitudes (N_θ), longitudes ($N_\phi = 2(N_\theta - 1)$), and modes in the radial direction (N_r), respectively.

5. Numerical results

In this section we present two sets of numerical experiments which illuminate the behavior of our new numerical scheme. The first is based upon an exact solution, cf. (30), which we have found useful in measuring the performance of Boundary Perturbation methods. The second set approximates our original plane-wave scattering problem; here highly resolved numerical simulations are used as reference solutions.

5.1. Computations of surface currents

To evaluate the performance of a numerical algorithm for scattering there are many tests, in both the near and far fields, available for consideration. As in [4] we choose to measure the normal derivative of the field at the scattering surface, cf. Section 3.1 and Fig. 1, which, for electromagnetics applications, has the physical interpretation of a current. We define this normal derivative as

$$v(\theta) := \nabla v|_{r=a+\varepsilon f} \cdot N_g,$$

where

$$\nabla v = \left(\partial_r v, \frac{1}{r} \partial_\theta v, \frac{1}{r \sin(\theta)} \partial_\phi v \right),$$

and

$$N_g := \left((a+g), -(\partial_\theta g), -\frac{1}{\sin(\theta)} \partial_\phi g \right)$$

is chosen unnormalized as in [4]. With this choice of normal it is easy to see that

$$v(\theta) = (a+g) \partial_r v|_{r=a+\varepsilon f} - \frac{(\partial_\theta g)}{(a+g)} \partial_\theta v|_{r=a+\varepsilon f} - \frac{(\partial_\phi g)}{(a+g) \sin^2(\theta)} \partial_\phi v|_{r=a+\varepsilon f}. \tag{32}$$

To use the TFE algorithm in a simulation of the current v, (32), we must perform a few manipulations:

$$(a+g)(d-g)v = (a+g)^2 (d-g) \partial_r v|_{r=a+g} - (\partial_\theta g)(d-g) \partial_\theta v|_{r=a+g} - \frac{1}{\sin^2(\theta)} (\partial_\phi g)(d-g) \partial_\phi v|_{r=a+g}$$

$$= (a+g)^2 d \partial_{r'} u|_{r'=a} - (\partial_{\theta'} g)(d-g) \partial_{\theta'} u|_{r'=a} + (\partial_{\theta'} g)^2 d \partial_{r'} u|_{r'=a} - \frac{1}{\sin^2(\theta)} (\partial_{\phi'} g)(d-g) \partial_{\phi'} u|_{r'=a}$$

$$+ \frac{1}{\sin^2(\theta)} (\partial_{\phi'} g)^2 d \partial_{r'} u|_{r'=a},$$

where we have used (14) to change coordinates. Dropping primes and further simplifying we find

$$(a+g)(d-g)v = (a+g)^2 d \partial_r u + d \partial_r u \left\{ (\partial_\theta g)^2 + \frac{1}{\sin^2(\theta)} (\partial_\phi g)^2 \right\} - (d-g) \left\{ (\partial_\theta g) \partial_\theta u + \frac{1}{\sin^2(\theta)} (\partial_\phi g) \partial_\phi u \right\}$$

$$= (a+g)^2 d \partial_r u + d \partial_r u \left\{ \mathscr{I} \left[\frac{1}{2} g^2 \right] - g \mathscr{I}[g] \right\} - \frac{1}{2} (d-g) \{ \mathscr{I}[gu] - g \mathscr{I}[u] - u \mathscr{I}[g] \}, \tag{33}$$

where u is to be evaluated at $r=a$. Setting $g = \varepsilon f$, the current, v, in the new coordinates is also analytic in ε [19], provided that f is sufficiently smooth, so that

$$v(\theta, \phi, \varepsilon) = \sum_{n=0}^{\infty} v_n(\theta, \phi) \varepsilon^n,$$

and (33) can be used to show that

$$a\, d\, v_n = (a-d)f v_{n-1} + f^2 v_{n-2} + a^2 d\, \partial_r u_n + 2adf\, \partial_r u_{n-1} + f^2 d\, \partial_r u_{n-2} + d\mathscr{I}\left[\frac{1}{2}f^2\right]\partial_r u_{n-2} - df\mathscr{I}[f]\partial_r u_{n-2}$$

$$- \frac{1}{2}d\mathscr{I}[f u_{n-1}] + \frac{1}{2}df\mathscr{I}[u_{n-1}] + \frac{1}{2}d\mathscr{I}[f]u_{n-1} + \frac{1}{2}f\mathscr{I}[f u_{n-2}] - \frac{1}{2}f^2\mathscr{I}[u_{n-2}] - \frac{1}{2}f\mathscr{I}[f]u_{n-2},$$

where terms with negative index are set to zero. From this we can approximate v with

$$v_N(\theta', \phi', \varepsilon) := \sum_{n=0}^{N} v_n(\theta', \phi')\varepsilon^n. \tag{34}$$

Before discussing our numerical results in detail, we point out that the Taylor series (34) evaluated at a particular point (θ_0', ϕ_0') may be summed directly ("Taylor summation"), or rationally approximated using the method of Padé [28]. To summarize this method, suppose that the truncated Taylor series

$$t^N(\varepsilon) := \sum_{n=0}^{N} t_n \varepsilon^n$$

of an analytic function $t(\varepsilon)$ is approximated by the rational function

$$p^{L,M}(\varepsilon) := \frac{\sum_{l=0}^{L} a_l \varepsilon^l}{\sum_{m=0}^{M} b_m \varepsilon^m},$$

where $L + M = N$ and the $\{a_l, b_m\}$ are determined from the $\{t_n\}$ via Padé's algorithm [28]. Then $p^{L,M}(\varepsilon)$ has rather remarkable properties of approximation of $t(\varepsilon)$, in particular, the ability to deliver, with high accuracy, the value of $t(\varepsilon_0)$ when ε_0 is a point of analyticity *outside* the disk of convergence of the Taylor series of $t(\varepsilon)$ [28]. As we shall later see, this enables us to compute scattering returns from obstacles which are very *large* perturbations of a circle.

5.2. Exact solutions

As we saw at the end of Section 4, a useful family of exact solutions of (9a) and (9c) is given by the $U_{l,m}$ of (30) for each (l,m). Given a profile $g(\theta, \phi) = \varepsilon f(\theta, \phi)$ we will have a solution to (9) provided that we set

$$\xi(\theta, \phi) = \xi_{l,m}(\theta, \phi) := U_{l,m}(a + \varepsilon f(\theta, \phi), \theta, \phi). \tag{35}$$

So, provided with the triple $(\varepsilon, f, \xi_{l,m})$, the TFE algorithm delivers approximations to the field and the current which can be compared with the *exact* field, $U_{l,m}$, and its current. For the experiments of this section we will choose the nondimensional radius $a = 1$, together with $b = 2$, $l = 2$, and $m = 1$. Regarding the profiles, f, which specify the perturbation of the scatterer from a sphere, we choose the shapes considered by Bruno and Reitich [6]:

$$f_1(\theta, \phi) = \frac{3}{2}\cos^2(\theta) - \frac{1}{2}, \tag{36a}$$

$$f_2(\theta, \phi) = \frac{1}{8}(35\cos^4(\theta) - 30\cos^2(\theta) + 3), \tag{36b}$$

$$f_3(\theta, \phi) = \frac{3}{8}\cos(\phi)\sin(\theta)(4 - 5\sin^2(\theta)). \tag{36c}$$

For each profile we conduct the following tests:

(1) Fixing the frequency $k = 1$ we vary ε to demonstrate the robustness with respect to the perturbation size.
(2) Fixing the perturbation size $\varepsilon = 0.1$ we vary the frequency k to demonstrate the robustness with respect to the frequency.

For the first profile f_1 given in (36a) and pictured in Fig. 3, we show, in Fig. 4, the results as ε is varied through values of 0.125, 0.25, 0.5, and 1.0 for $k = 1$. Here the errors are dominated by the expansion error.
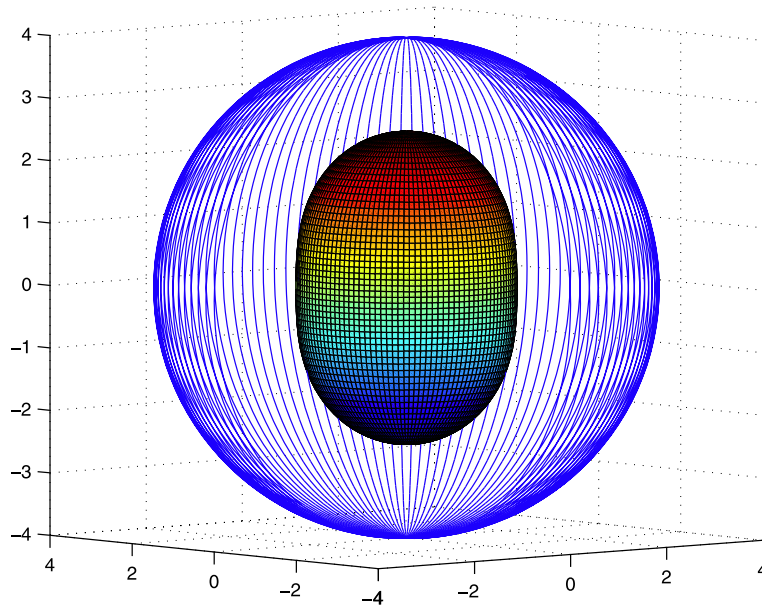
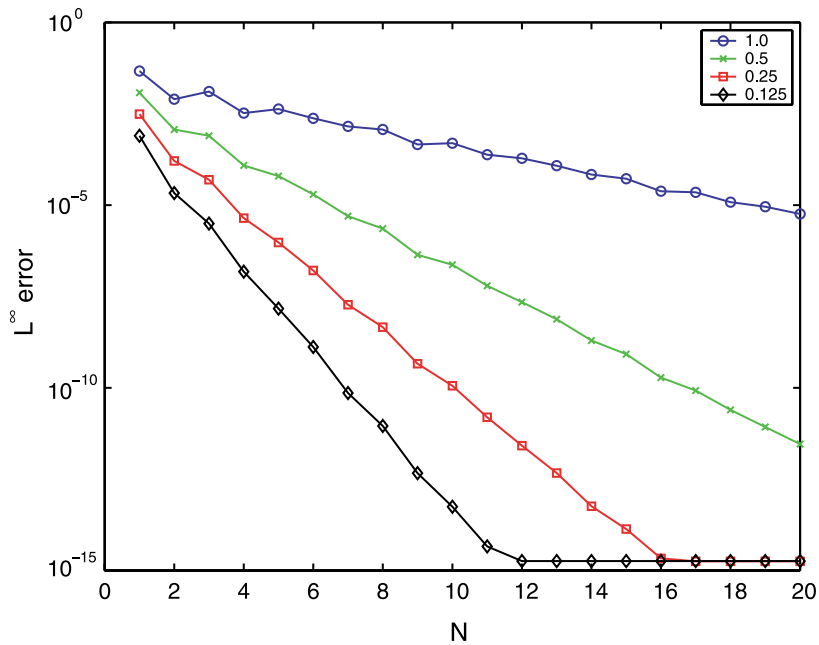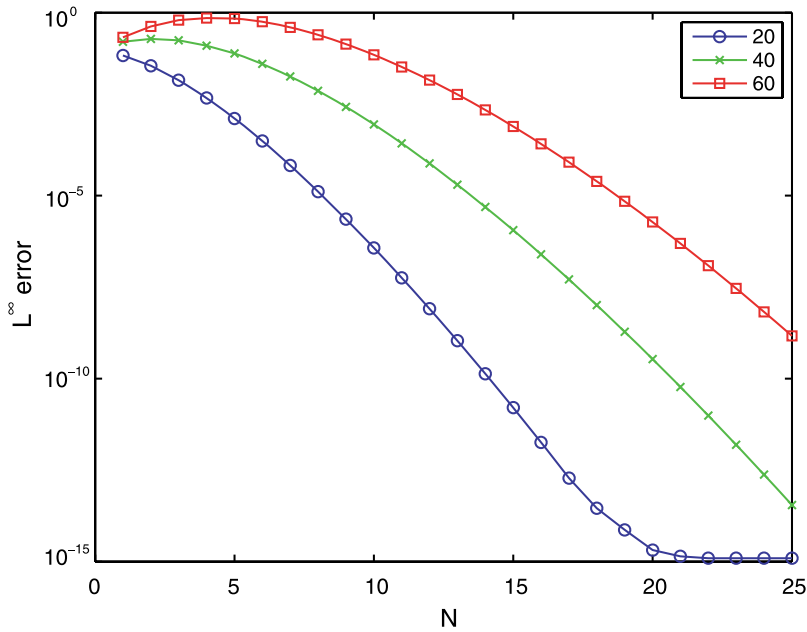Fig. 3. Domain shaped by f_1, cf. (36a), with $\varepsilon = 0.5$.

Fig. 4. Error in current, measured in L^∞, between an exact solution, (30), and our new TFE algorithm. The scattering obstacle is shaped by $r = 1 + \varepsilon f_1$. The frequency is fixed at $k = 1$, the perturbation amplitudes are $\varepsilon = 0.125, 0.25, 0.5, 1.0$, and the numerical parameters are $N_\theta = 40$, $N_\phi = 78$, and $N_r = 60$.

We observe that the errors decay monotonically as N, the number of terms in the perturbation expansion, increases. It is remarkable that the algorithm even converges at the very large value of $\varepsilon = 1$ thanks to the use of Padé summation.

Fig. 5. Error in current, measured in L^∞, between an exact solution, (30), and our new TFE algorithm. The scattering obstacle is shaped by $r = 1 + \varepsilon f_1$. The perturbation amplitude is fixed at $\varepsilon = 0.1$, the frequencies are $k = 20, 40, 60$, and the numerical parameters are $N_\theta = 50$, $N_\phi = 98$, and $N_r = 60$.

In Fig. 5, we fix $\varepsilon = 0.1$ and show the convergence results for frequencies $k = 20, 40, 60$. We observe that the error decays monotonically as N increases until it reaches machine precision or the accuracy limited by the spatial resolution. We note that even at a relatively high frequency $k = 60$, the modest number of modes used in this test still provide very accurate results.

Remark 3. Before we move to the other two profiles, let us point out another advantage of our approach. Since we use a spectral approximation of the exact Dirichlet Neumann Operator, T, we can choose the outer boundary to be quite close to the obstacle, thus, reducing the *effective wave number* in the radial direction from $(a + |g|_{L^\infty})k$ to essentially $(|g|_{L^\infty})k$, and consequently, reducing the required number of points in the radial direction significantly.

In order to validate the above claim, we fix $\varepsilon = 0.1$, $N_\theta = 50$ and $N_\phi = 98$ and we compare the errors in choosing $b = 2$ as compared to $b = 1.2$ with three frequencies and two values of N_r. The results are reported in Table 1. We observe, for example, that for $b = 2$ and $k = 40$, $N_r = 50$ is required for the error to be of order 10^{-13} while only $N_r = 24$ is needed if we choose $b = 1.2$. Clearly, one should choose b to be very close to $(a + |g|_{L^\infty})$ to minimize the number of modes needed in the radial direction.

Now we consider the second profile f_2 given in (36b) and shown in Fig. 6. We present in Fig. 7 the results as ε is varied through values of 0.125, 0.25 and 0.5 for $k = 1$. The error behavior is similar to that for the first profile except that slightly more terms in the Taylor series are needed as this profile is a more irregular deformation of the sphere. In Fig. 8, we present the convergence results for frequencies $k = 20, 40, 60$ with $\varepsilon = 0.1$. The results are, again, similar to the first case save that a few more modes were necessary to achieve comparable accuracy.

We now turn to the third profile f_3 given in (36c) and pictured in Fig. 9. In Fig. 10, the results with fixed parameters $k = 1$, $N_\theta = 40$, $N_\phi = 78$, and $N_r = 60$ are shown for varying ε. In Fig. 11, we report the convergence results for frequencies $k = 20, 40, 60$ with $\varepsilon = 0.1$ and $N_\theta = 50$, $N_\phi = 98$, $N_r = 60$. These results are also very similar to the first two profiles, except that in Fig. 11, the plateau reached at $N = 21$ for $k = 60$ is due to insufficient spatial resolution.

Table 1
Comparison of errors with $b = 2$ and $b = 1.2$

N_r	$k = 20$	$k = 40$	$k = 60$
Case I. $a = 1$, $b = 2$			
20	$0.29763838 \times 10^{-6}$	N/A	N/A
30	$0.33960572 \times 10^{-13}$	$0.67513035 \times 10^{-5}$	N/A
40	$0.15703991 \times 10^{-14}$	$0.46352098 \times 10^{-10}$	$0.88338883 \times 10^{-3}$
50	$0.17613860 \times 10^{-14}$	$0.34953493 \times 10^{-13}$	$0.36524574 \times 10^{-7}$
60	$0.12354349 \times 10^{-14}$	$0.35001966 \times 10^{-13}$	$0.14695808 \times 10^{-8}$
Case II. $a = 1$, $b = 1.2$			
10	$0.17356540 \times 10^{-7}$	$0.26397995 \times 10^{-4}$	N/A
16	$0.50100256 \times 10^{-14}$	$0.49344552 \times 10^{-9}$	$0.71672433 \times 10^{-3}$
24	$0.22039046 \times 10^{-14}$	$0.58447350 \times 10^{-13}$	$0.24197446 \times 10^{-8}$
32	$0.22163657 \times 10^{-14}$	$0.58473324 \times 10^{-13}$	$0.25240995 \times 10^{-8}$
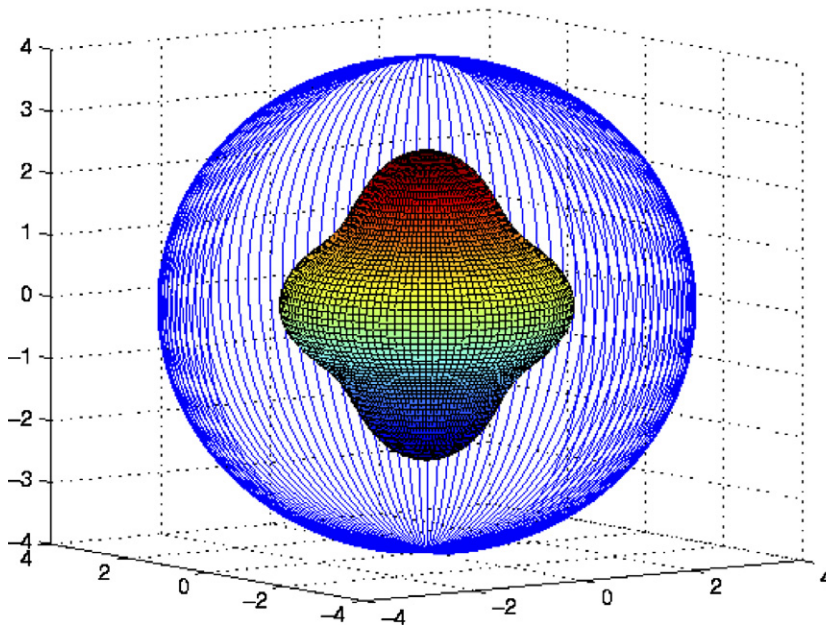
Fig. 6. Domain shaped by f_2, cf. (36b), with $\varepsilon = 0.5$.

5.3. Plane-wave scattering

In the experiments described in this section we return to the original plane-wave scattering problem (5) with the Dirichlet data ξ set equal to the opposite of the incident radiation, (1), evaluated at the surface of the scatterer. We will choose the problem parameters $a = 1$, $b = 2$, and the profiles f_1, f_2, and f_3 from Section 5.2. Of course, we no longer have an exact solution for comparison and instead use a "high resolution" approximation ($N_\theta = 81$, $N_\phi = 140$, $N_r = 80$) as a reference solution.

Beginning with the profile f_1, (36a) (see Fig. 3) with perturbation size $\varepsilon = 0.1$ we display in Fig. 12 results of numerical simulations with frequencies $k = 1, 5, 10, 20$. In this example the numerical parameters are set to $N_\theta = 41$, $N_\phi = 70$, $N_r = 60$. We point out that by order $N = 13$ we can achieve "best" accuracies (allowed by the fixed spatial resolution) of 10^{-14}, 10^{-12}, 10^{-9} and 10^{-6} for $k = 1, 5, 10$ and 20, respectively. To achieve better results naturally requires a further refinement of the numerical parameters N_θ, N_ϕ, and N_r.
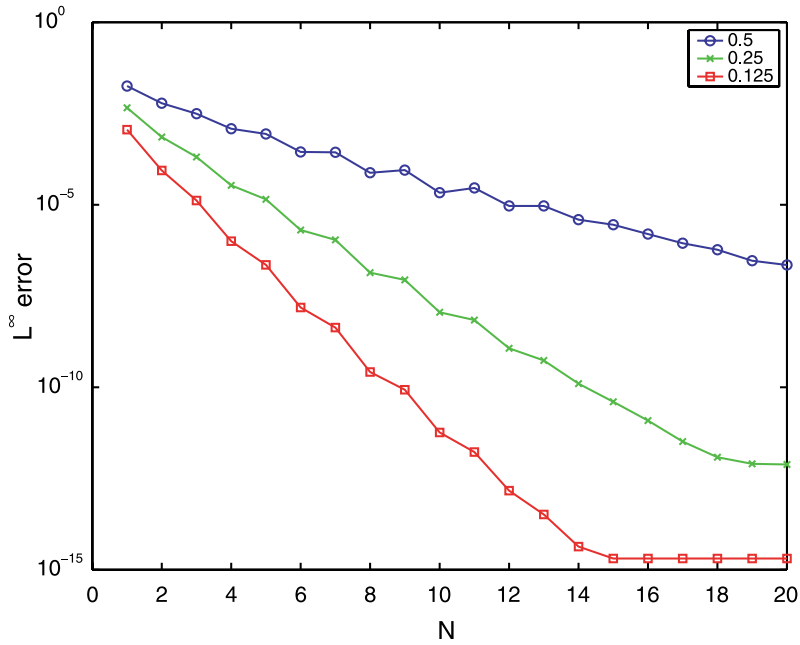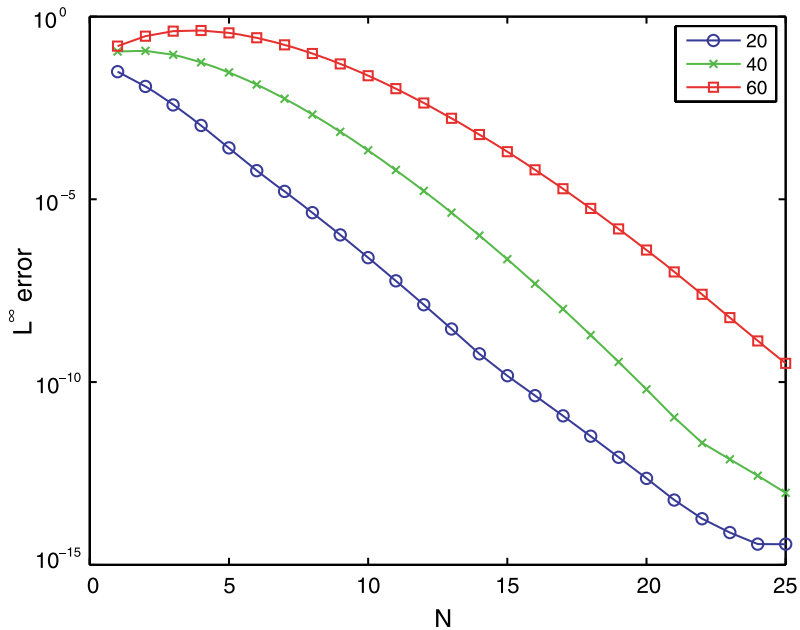
Fig. 7. Error in current, measured in L^∞, between an exact solution, (30), and our new TFE algorithm. The scattering obstacle is shaped by $r = 1 + \varepsilon f_2$. The frequency is fixed at $k = 1$, the perturbation amplitudes are $\varepsilon = 0.125, 0.25, 0.5$, and the numerical parameters are $N_\theta = 40$, $N_\phi = 78$, and $N_r = 60$.

Fig. 8. Error in current, measured in L^∞, between an exact solution, (30), and our new TFE algorithm. The scattering obstacle is shaped by $r = 1 + \varepsilon f_2$. The perturbation amplitude is fixed at $\varepsilon = 0.1$, the frequencies are $k = 20, 40, 60$, and the numerical parameters are $N_\theta = 70$, $N_\phi = 138$, and $N_r = 60$.
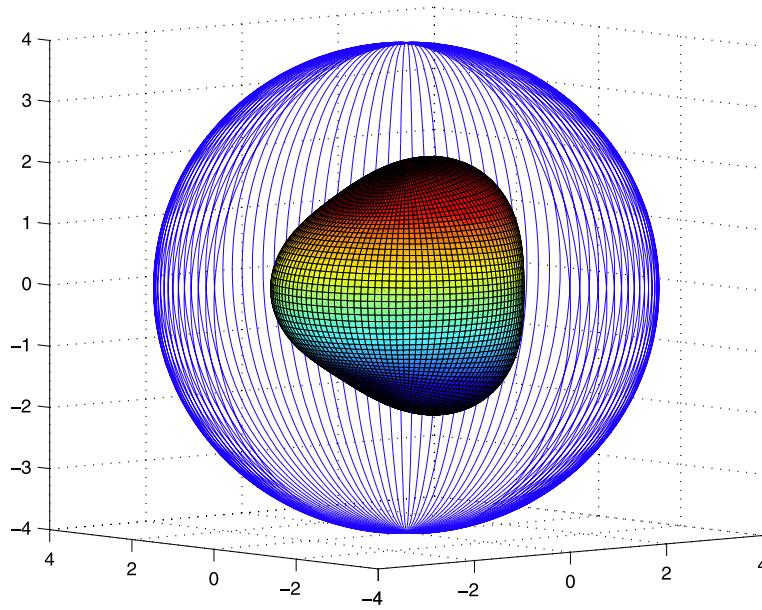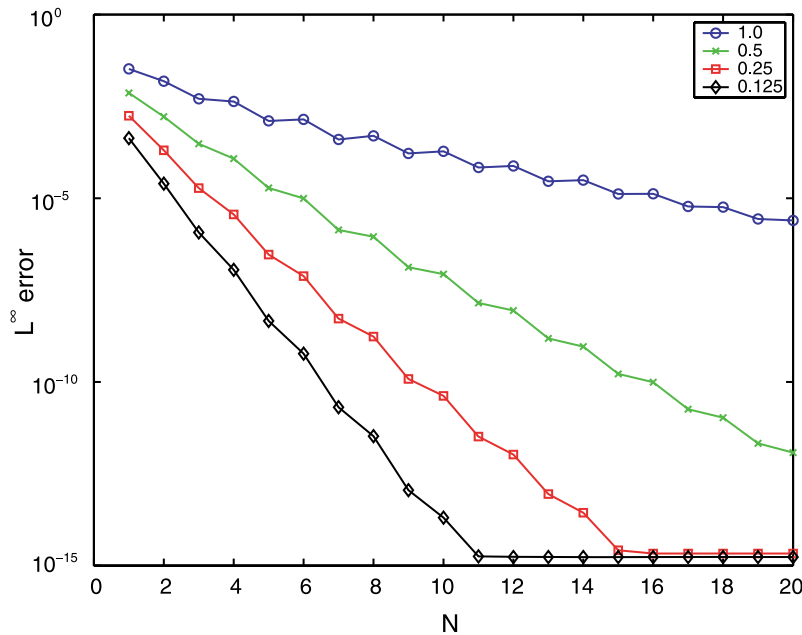
Fig. 9. Domain shaped by f_3, cf. (36c), with $\varepsilon = 0.5$.

Fig. 10. Error in current, measured in L^∞, between an exact solution, (30), and our new TFE algorithm. The scattering obstacle is shaped by $r = 1 + \varepsilon f_3$. The frequency is fixed at $k = 1$, the perturbation amplitudes are $\varepsilon = 0.125, 0.25, 0.5, 1.0$, and the numerical parameters are $N_\theta = 40$, $N_\phi = 78$, and $N_r = 60$.

In Figs. 13 and 14 we display similar results for the profiles f_2, (36b), and f_3, (36c). Again, the perturbation size is fixed at $\varepsilon = 0.1$ while the frequencies are varied through $k = 1, 5, 10, 20$. The numerical parameters are fixed at $N_\theta = 41$, $N_\phi = 70$, $N_r = 60$. We note that the "best" accuracies, allowed by the fixed spatial resolution,
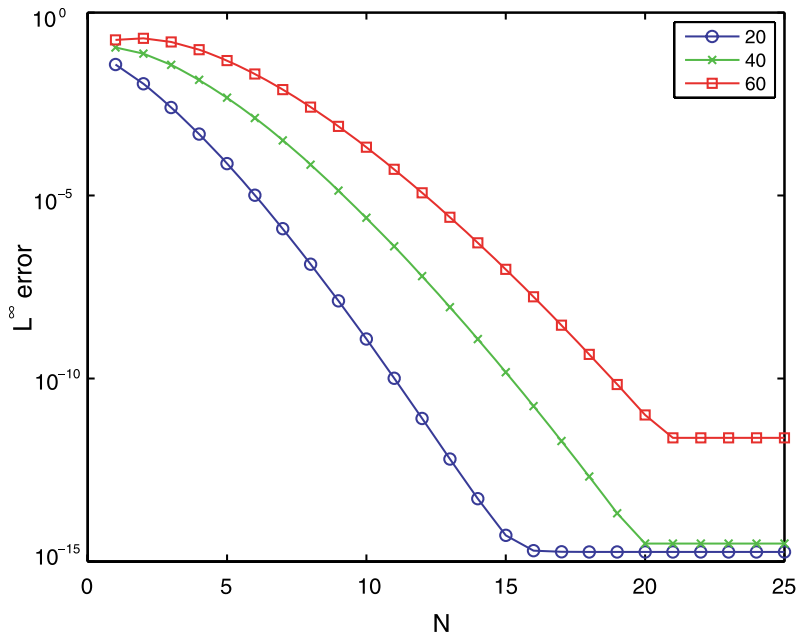
Fig. 11. Error in current, measured in L^∞, between an exact solution, (30), and our new TFE algorithm. The scattering obstacle is shaped by $r = 1 + \varepsilon f_3$. The perturbation amplitude is fixed at $\varepsilon = 0.1$, the frequencies are $k = 20, 40, 60$, and the numerical parameters are $N_\theta = 50$, $N_\phi = 98$, and $N_r = 60$.

can be achieved for all frequencies considered by $N = 16$ (for f_2) and $N = 13$ (for f_3). The precise values of these accuracies is determined by the numerical parameters and can be further reduced with refinement in the discretization parameters N_θ, N_ϕ, and N_r.
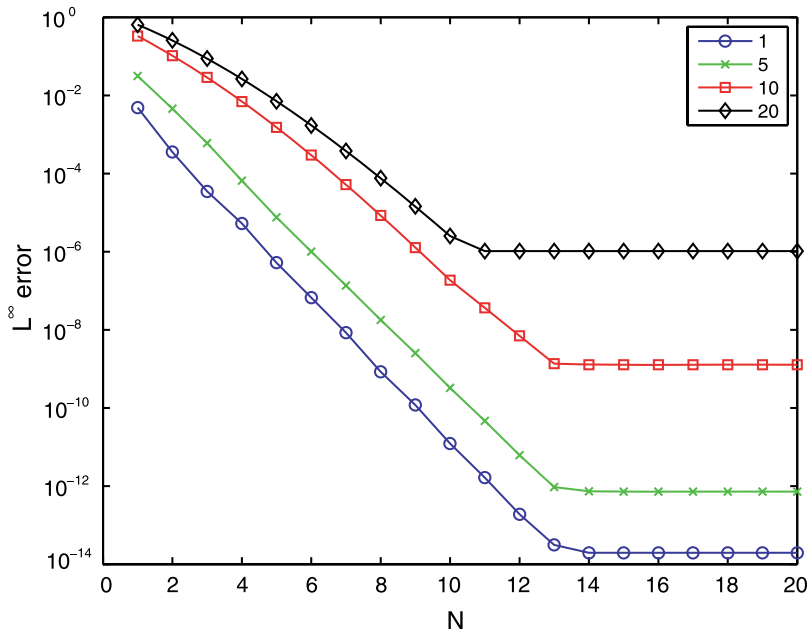

Fig. 12. Error in current, measured in L^∞, between a highly resolved plane-wave solution, and our new TFE algorithm. The scattering obstacle is shaped by $r = 1 + \varepsilon f_1$. The perturbation amplitude is fixed at $\varepsilon = 0.1$, the frequencies are $k = 1, 5, 10, 20$, and the numerical parameters are $N_\theta = 41$, $N_\phi = 70$, and $N_r = 60$.
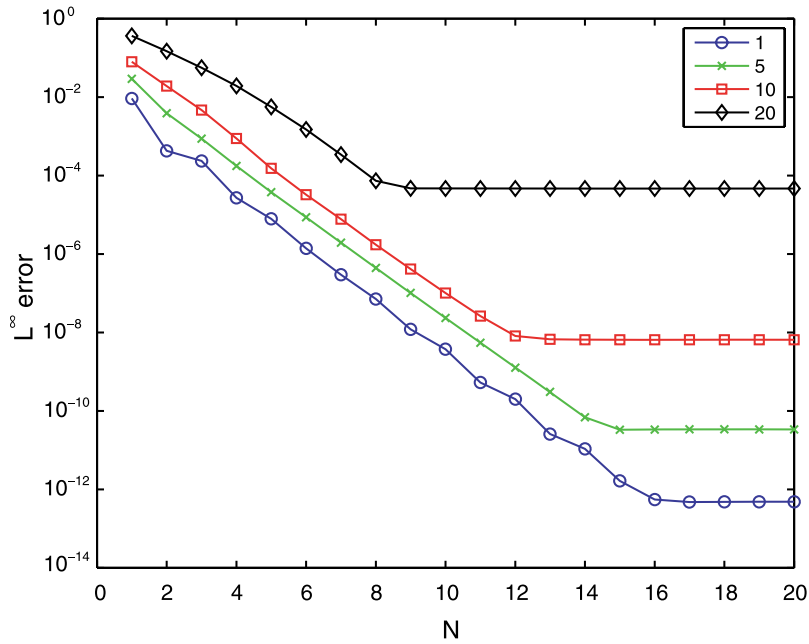
Fig. 13. Error in current, measured in L^∞, between a highly resolved plane-wave solution, and our new TFE algorithm. The scattering obstacle is shaped by $r = 1 + \varepsilon f_2$. The perturbation amplitude is fixed at $\varepsilon = 0.1$, the frequencies are $k = 1, 5, 10, 20$, and the numerical parameters are $N_\theta = 41$, $N_\phi = 70$, and $N_r = 60$.
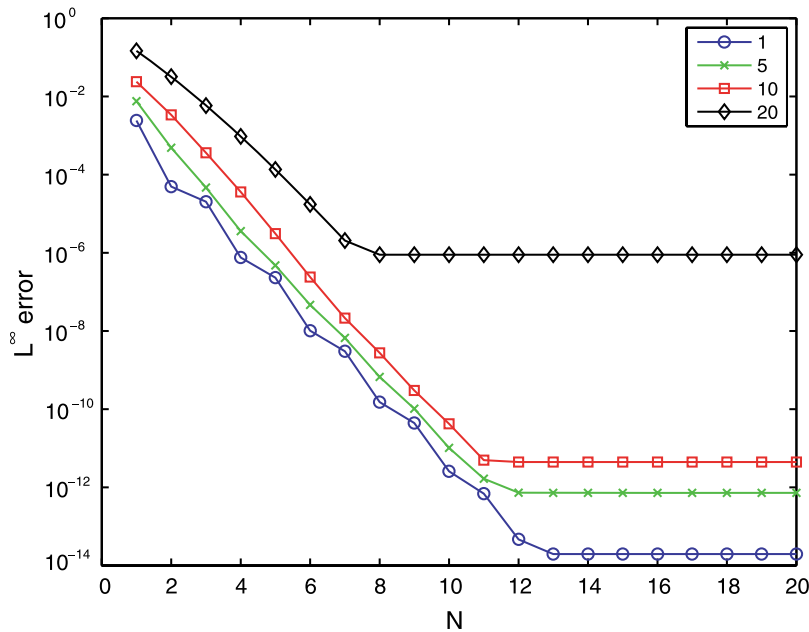

Fig. 14. Error in current, measured in L^∞, between a highly resolved plane-wave solution, and our new TFE algorithm. The scattering obstacle is shaped by $r = 1 + \varepsilon f_3$. The perturbation amplitude is fixed at $\varepsilon = 0.1$, the frequencies are $k = 1, 5, 10, 20$, and the numerical parameters are $N_\theta = 41$, $N_\phi = 70$, and $N_r = 60$.

6. Concluding remarks

In this paper, we have presented an efficient and high-order algorithm for three-dimensional bounded obstacle acoustic scattering. The method extends our recent work [4] for two-dimensional bounded obstacle scattering, and is based upon a boundary perturbation method paired with a high-order spectral-Galerkin solver. This boundary perturbation approach is justified by rigorous theoretical results on analyticity of the scattered field with respect to boundary variations. Several numerical results have been presented to exemplify the accuracy, stability, and versatility of the proposed method.

References

[1] D. Colton, R. Kress, Inverse Acoustic and Electromagnetic Scattering Theory, second ed., Springer, Berlin, 1998.
[2] K.F. Warnick, W.C. Chew, Numerical simulation methods for rough surface scattering, Waves Random Media 11 (1) (2001) R1–R30.
[3] F. Reitich, K. Tamma, State-of-the-art, trends, and directions in computational electromagnetics, CMES Comput. Model. Eng. Sci. 5 (4) (2004) 287–294.
[4] D.P. Nicholls, J. Shen, A stable, high-order method for two-dimensional bounded-obstacle scattering, SIAM J. Sci. Comput. 28 (4) (2006) 1398–1419.
[5] O.P. Bruno, C.A. Geuzaine, J.A. Munro, F. Reitich, Prescribed error tolerances within fixed computational times for scattering problems of arbitrarily high frequency: The convex case, Philos. Trans. R. Soc. Lond. A 362 (2004) 629–645.
[6] O.P. Bruno, F. Reitich, Boundary-variation solutions for bounded-obstacle scattering problems in three dimensions, J. Acoust. Soc. Am. 104 (5) (1998) 2579–2583.
[7] L. Rayleigh, On the dynamical theory of gratings, Proc. R. Soc. London A 79 (1907) 399–416.
[8] S.O. Rice, Reflection of electromagnetic waves from slightly rough surfaces, Commun. Pure Appl. Math. 4 (1951) 351–378.
[9] O.P. Bruno, F. Reitich, Numerical solution of diffraction problems: a method of variation of boundaries, J. Opt. Soc. Am. A 10 (6) (1993) 1168–1175.
[10] O.P. Bruno, F. Reitich, Numerical solution of diffraction problems: a method of variation of boundaries. II. Finitely conducting gratings, Padé approximants, and singularities, J. Opt. Soc. Am. A 10 (11) (1993) 2307–2316.
[11] O.P. Bruno, F. Reitich, Numerical solution of diffraction problems: a method of variation of boundaries. III. Doubly periodic gratings, J. Opt. Soc. Am. A 10 (12) (1993) 2551–2562.
[12] O.P. Bruno, F. Reitich, Calculation of electromagnetic scattering via boundary variations and analytic continuation, Appl. Comput. Electromagn. Soc. J. 11 (1) (1996) 17–31.
[13] O.P. Bruno, F. Reitich, High-order boundary perturbation methods, Mathematical Modeling in Optical Science, Frontiers in Applied Mathematics Series, vol. 22, SIAM, Philadelphia, PA, 2001, pp. 71–109.
[14] D.P. Nicholls, F. Reitich, A new approach to analyticity of Dirichlet-Neumann operators, Proc. R. Soc. Edinburgh A 131 (6) (2001) 1411–1433.
[15] D.P. Nicholls, F. Reitich, Shape deformations in rough surface scattering: cancellations, conditioning, and convergence, J. Opt. Soc. Am. A 21 (4) (2004) 590–605.
[16] D.P. Nicholls, F. Reitich, Shape deformations in rough surface scattering: improved algorithms, J. Opt. Soc. Am. A 21 (4) (2004) 606–621.
[17] D.P. Nicholls, F. Reitich, Stability of high-order perturbative methods for the computation of Dirichlet–Neumann operators, J. Comput. Phys. 170 (1) (2001) 276–298.
[18] D.P. Nicholls, F. Reitich, Analytic continuation of Dirichlet–Neumann operators, Numer. Math. 94 (1) (2003) 107–146.
[19] D.P. Nicholls, N. Nigam, Exact non-reflecting boundary conditions on general domains, J. Comput. Phys. 194 (1) (2004) 278–303.
[20] R. Suda, M. Takami, A fast spherical harmonics transform algorithm, Math. Comp. 71 (238) (2002) 703–715 (electronic).
[21] D.P. Nicholls, F. Reitich, On analyticity of traveling water waves, Proc. R. Soc. London A 461 (2057) (2005) 1283–1309.
[22] I. Harari, T.J.R. Hughes, Analysis of continuous formulations underlying the computation of time-harmonic acoustics in exterior domains, Comput. Methods Appl. Mech. Eng. 97 (1) (1992) 103–124.
[23] L. Demkowicz, F. Ihlenburg, Analysis of a coupled finite-infinite element method for exterior Helmholtz problems, Numer. Math. 88 (1) (2001) 43–73.
[24] J. Shen, Efficient spectral-Galerkin method. I. Direct solvers of second- and fourth-order equations using Legendre polynomials, SIAM J. Sci. Comput. 15 (6) (1994) 1489–1505.
[25] J. Shen, Efficient spectral-Galerkin method. II. Direct solvers of second- and fourth-order equations using Chebyshev polynomials, SIAM J. Sci. Comput. 16 (1) (1995) 74–87.
[26] J. Shen, L.-L. Wang, Analysis of spectral approximation to the Helmholtz equation in exterior domains (submitted).
[27] J. Shen, L.-L. Wang, Spectral approximation of the Helmholtz equation with high wave numbers, SIAM J. Numer. Anal. 43 (2) (2005) 623–644.
[28] G.A. Baker Jr., P. Graves-Morris, Padé approximants, second ed., Cambridge University Press, Cambridge, 1996.